Hearty Paul (Orcid ID: 0000-0002-6976-3546)
Rovere Alessio (Orcid ID: 0000-0001-5575-1168)
O'Leary Michael, J (Orcid ID: 0000-0001-7040-3137)
Raymo Maureen (Orcid ID: 0000-0001-7967-9105)

Pliocene-Pleistocene stratigraphy and sea-level estimates, Republic of South Africa with implications for a 400 ppmv CO_2 world

PJ Hearty[1], A Rovere[2,3], MR Sandstrom[3], MJ O'Leary[4], D. Roberts[5†], ME Raymo[3]

[1] Department of Geological Sciences, Jackson School of Geosciences, The University of Texas at Austin, 1 University Station, C1100, Austin, TX 78712-0254 USA

[2] MARUM, University of Bremen and ZMT, Leibniz Center for Tropical Marine Ecology, Germany, Germany

[3] Lamont-Doherty Earth Observatory, Columbia University, Palisades, NY, 10964 USA.

[4] Centre for Energy Geoscience, School of Earth Sciences, The University of Western Australia, Perth, Western Australia 6009

[5] Council for Geosciences, Cape Town and Faculty of Natural and Agricultural Sciences, University of the Free State, 205 Nelson Mandela Drive, Bloemfontein, 9300, Republic of South Africa.

Corresponding author: Paul J. Hearty (kaisdad04@gmail.com)

†Deceased 9/2015.

Key Points:

- The relative tectonic stability of South Africa provides an optimal location for study of sea-level history
- There is an abundance of excellent Pliocene and Pleistocene (5-1 Ma) marine exposures along the semi-arid coastlines
- Precise measurements of these sea-level indicators provide significant implications for the historical rise in CO_2 levels above 400 ppmv

This article has been accepted for publication and undergone full peer review but has not been through the copyediting, typesetting, pagination and proofreading process which may lead to differences between this version and the Version of Record. Please cite this article as doi: 10.1029/2019PA003835

Abstract

The Mid-Pliocene Warm Period (MPWP, 2.9 to 3.3 Ma), along with older Pliocene (3.2 to 5.3 Ma) records, offers potential past analogues for our 400-ppmv world. The coastal geology of western and southern coasts of the Republic of South Africa expose an abundance of marine deposits of Pliocene and Pleistocene age. In this study, we report differential GPS elevations, detailed stratigraphic descriptions, standardized interpretations, and dating of relative sea-level indicators measured across ~700 km from the western and southern coasts of the Cape Provinces. Wave abrasion surfaces on bedrock, intertidal sedimentary structures, and *in situ* marine invertebrates including oysters and barnacles provide precise indicators of past sea levels. Multiple sea-level highstands imprinted at different elevations along South African coastlines were identified. Zone I sites average +32 ± 5 m (6 sites). A lower topographic Zone II of sea stands were measured at several sites around +17 ± 5 m. Middle and late Pleistocene sites are included in Zone III. Shoreline chronologies using $^{87}Sr/^{86}Sr$ ages on shells from these zones yield ages from Zone I at 4.6 and 3.0 Ma, and Zone II at 1.04 Ma. Our results show that polar ice sheets during the Plio-Pleistocene were dynamic and subject to significant melting under modestly warmer global temperatures. These processes occurred during a period when CO_2 concentrations were comparable to our current and rapidly rising values above 400 ppmv.

Plain Language Summary

The ancient coastal deposits of the Republic of South Africa provide an opportunity to examine past climatic effects on ice sheets and sea levels during the Pliocene. This was the last time atmospheric CO_2 was similar to our current and rising level of ~415 ppmv. Indicators of past sea levels were measured at a number of natural rock outcrops that date between about 1 and 5 million years old. Our studies have found that average sea levels ranged between 15 and 30 m higher than present. Post-depositional effects by crustal movements caused by plate tectonics or ice sheets are minor but have yet to be fully quantified. Regardless, our baseline field data have important implications for the magnitude of our present and future climate and sea-level changes.

1 Introduction

The rapid rise in atmospheric CO_2 to levels exceeding 400 ppmv (Monastersky, 2013) is driving an urgent need to better understand sea-level changes and ice sheet dynamics associated with past warmer-than-present geological intervals. The Mid-Pliocene Warm Period (MPWP; 3.3 to 2.9 Ma), and indeed most of the Pliocene, was the last time Earth experienced CO_2 levels around or above 400 ppmv (Pagani et al., 2010; Stap et al., 2016; Fischer et al., 2018). As such, the Pliocene may serve as an analogue for the Earth's near future climate changes. Understanding the potential response of Greenland and Antarctic ice sheets to Earth warming is critical, as there is strong evidence from modeling studies that the ocean-cryosphere system is dynamic (e.g., DeConto and Pollard, 2016; Pollard and DeConto, 2009; Pollard et al. 2015) and could lead to rapid ice collapse and global sea-level rise in this century (Golledge et al., 2019).

The measurement, interpretation and dating of RSL indicators is essential to derive more accurate estimates of eustatic sea-level (ESL) highstands during the Plio-Pleistocene and the related loss of polar ice. In this paper, we present the results of extensive field mapping along different coastal sectors of the Republic of South Africa (hereafter RSA, see map in Figure 1). The primary objective of our study was to characterize high-resolution sea-level stratigraphic sections. Integral to establishing RSL and indicative meaning, is a clear understanding and accurate interpretation of the sedimentary facies and stratigraphic succession (as illustrated, for example, in Figure 4) along the coastline. Once optimal field samples from key sites were collected, ages were determined using $^{87}Sr/^{86}Sr$ geochronological methods.

While the long-term uplift (Cretaceous to Cenozoic) history of the southern tip of the African continent is characterized by phases of uplift and quiescence (e.g., see Baby et al., 2019, Marker and Holmes, 2010, Dauteuil et al., 2015, Wahlford and White, 2005), the choice of RSA as study area resides in the fact that the intra-continental plate, trailing edge coastal margin of the southerly African Plate has been considered to be relatively tectonically stable throughout the Pliocene and Pleistocene (Roberts et al., 2012; Chen et al. 2014; Konouv et al., 2015). Data on linear inverse modelling of drainage networks showed that, in the Northern and Western Cape Provinces of RSA, average uplift rates for the last ca. 15 Ma were, on average, 0.011±0.02 mm/a.

For the RSA, glacial isostatic adjustment (GIA) models predict only slight departures from eustasy (Raymo et al. 2011; Rovere et al., 2014) and are characterized by relatively small uncertainties when different mantle viscosity profiles are used to predict GIA for Pleistocene and Pliocene time scales (Rovere et al., 2014). Also, Dynamic Topography (DT), which is recognized to cause significant uplift or subsidence at Pleistocene and Pliocene time scales even at passive margins (Moucha et al., 2008; Austermann et al., 2017), appears to have a minor yet, currently uncertain effects along the western and southwestern coasts of South Africa. Interpreted peak sea levels (i.e., reduced global ice volume) are indicated on the basis of $\delta^{18}O$ around 5.1 Ma (T7/T5), the "Climatic Optimum" at 4.0 to 4.4 Ma (CN5-Gi25), the "MPWP" at 3.25 Ma (M1) to 2.94 (G17), 2.75 Ma (G7), and 2.5 Ma (MS99?) (Lisiecki and Raymo (2005). More directly, Naish et al. (2009) have identified and dated glacial advances and retreats (high sea levels) from glacio-marine sediments around Antarctica, and provide direct chronological evidence of an obliquity dominated sea-level cyclicity during the Pliocene, parallel to we observe on the shoreline during the MPWP. In the geologic record of RSA, we *infer* that the highest, longest, and latest highstand events should be discernible in

the field during a generally declining sea-level succession from the Pliocene to the Pleistocene. Our inference, despite being largely unprovable (i.e., the older deposits are destroyed), is based on logic. It stands to reason that if broad terraces are formed, and sea level amplitude is only 10-20 m, that geomorphic surfaces must be reoccupied multiple times – the "buzz saw" effect (see Discussion). Older deposits would be reworked and degraded; replaced by more recent ones.

2 Paleo sea level proxies in the Republic of South Africa – previous work

The study of coastal marine deposits in RSA expanded through the 20th Century, driven by the desire to document the evolution of large vertebrates (including hominids) on the continent of Africa, as well as exploration and exploitation of diamonds and other resources in coastal sedimentary deposits. Early works by Rogers (1905), Krige (1927), and later Siesser and Dingle (1981) provided a geological framework for many works to follow along the west coast of RSA. Krige's (1927) project embraced the entire South African coast. Coinciding with Krige's study, placer diamond deposits were found in sediments of the West Coast marine terraces, which spurred a surge of research bearing on their geomorphology, biostratigraphy and sedimentology (Haughton 1931) particularly in the area of Hondeklip Bay (see location in Figure 1B), in Namaqualand. This groundwork was later strengthened by Carrington and Kensley (1969), who expanded and integrated the knowledge of the biostratigraphy and chronology of these deposits. In particular they focused on the use of marine marker fossils as biostratigraphic indicators (mainly the bivalves *Isognomon* sp. the surf clam *Donax* sp., and the limpet *Fissurella* sp.) to distinguish and correlate sea-level events. Terraces of marine origin at elevations around 90 m (not further addressed), 50 m, 30 m and 18 m were previously described along the west coast of RSA (Roberts and Brink, 2002) and more recently, further north in Namibia (Stollhofen et al., 2014; Dauteuil et al., 2015; Zhu, 2016). Hereafter, we provide a brief account of the levels of marine terraces that are described in the literature.

2.1 Marine terraces at 50 m, 30 m and 21-18 m

Pickford (1998) interpreted what he defined as a "50 m Package" (i.e., a terrace level containing shell accumulations) to be late Miocene to earliest Pliocene (7-5 Ma) based on mammal fossils "similar" to those from Langebaanweg (Roberts et al., 2011). Pickford (1998) further correlated a series of lower terraces, which included a "30-m Package", with the Plio-Pleistocene between 3-2.5 Ma. This correlation was based in part on the presence of Equus, species of which colonized the Old World including Africa during the late Pliocene after about 3.4 Ma (Lindsay et al., 1980; Forstén, 1992; Jónsson et al., 2014).

Molluscan "zone fossils" in marine deposits from these terrace levels were similarly used to distinguish events during the Plio-Pleistocene, particularly making use of mollusk bivalve shells of the genus Donax. Carrington and Kensley (1969) correlated D. haughtoni with a "45-50 m strand line" where this taxon occurs "…in extraordinary abundance." The thicker and wider shell of D. rogersi is instead found in younger and lower marine deposits that Carrington and Kensley (1969) considered as Pleistocene in age.

Carrington and Kensley (1969) found evidence for temporally distinct marine transgressions of ~30 and ~20 m in excavations at Hondeklip Bay, and both levels contained the zone fossil D. rogersi. They considered these shorelines to be early-mid Pleistocene in age. Pether (1986 a,b; 1994 a,b) regarded the evidence for the +20-m level as spurious and recognized only the "30 m Package."

More recently, Roberts et al. (2011) summarized the Pliocene stratigraphy in the context of the stratigraphy and paleontology of Langebaanweg, a site located in the West Coast National Park. At this site, we have further documented the major units and the differential GPS (hereafter dGPS) elevations of their stratigraphic boundaries. The phosphatic deposits of the upper Varswater Formation contain marine microfossils (Dale and McMillan, 1999) that are regarded as marine/estuarine in origin at +30.7 m (elevation measured by our dGPS), and suggest the proximity of paleo-sea level during deposition (Hendey, 1981 a,b; 1983). Various authors suggest the rich vertebrate fossil deposits at Langebaanweg originate from a relative sea-level highstand peaking at 50 m the Early Pliocene around 5.5 to 4.8 Ma (vis-à-vis Pickford 1998), while the 30-m terrace is suspected to correlate with a Plio-Pleistocene transition after 3.3 Ma (Roberts et al., 2011).

Key marine biostratigraphic fossil indicators have been used to distinguish sea-level events of the Miocene and Pliocene. During our investigation, we only documented marine deposits or terrace landforms below +50 m. In our results section, we describe key sites yielding information on past relative sea levels that we surveyed at elevations between +41 and +10 m, which are the basis for the following results and discussion.

2.2 MIS 5e and MIS 11 RSL indicators

The measured elevation of younger Quaternary sea-level highstands (i.e., MIS 5e and MIS 11) in RSA provide important benchmarks on long-term vertical land motions. In the Western Cape Province, Carr et al. (2010) report deposits dated to MIS 5e from Swartvlei and Groot Brak estuaries (respectively located at 81 and 130 km from Still Bay (see location in Figure 1F) suggesting that the highstand was between +6 and +8.5 m above present sea level. These elevations do not change much further East. In fact, at a locality close to Nahoon River (620 km east of Still Bay), Jacobs and Roberts (2009) report a "*Shelly, Pebbly beachrock*" between +2.5 and +6 m above present sea level, dated to 117.3±6.2 ka with optically stimulated luminescence (their sample NHN1). At Cape Agulhas, Carr et al. (2010) (see location in Figure 1E) surveyed a gravel beach and an overlying sandy shoreface facies at elevations up to +7.5 m. These facies were dated to 118±7.2 ka with optically stimulated luminescence. At Hoë Walle, 35 km West of Cape Agulhas, the same authors report an aeolianite at +4 m dated 104±7 ka. Aeolianites few meters above sea level at Kraal Bay (130 km North of Cape Town and ca. 25 km South of Saldanha, see Figure 1D for location) were also attributed to MIS 5e (see Roberts, 2008 for details). These elevations of RSA MIS 5e sea levels are in general agreement with global averages (Hearty et al., 2007; O'Leary et al., 2013; Kopp et al. 2009).

Roberts et al. (2012) documented a MIS 11 sea stand at +13 m, subsequently corrected to account for GIA to a range of +8-11.5 m (Chen et al., 2014). These estimates of MIS 11 sea level are in general agreement with Bermuda, now dGPS surveyed at +18.3 m (Hearty et al., 1999; Olson and Hearty, 2009) later GIA corrected to +9-14 m (Raymo and Mitrovica, 2012) to take into account the location of Bermuda on the forebulge of the former Laurentide ice sheet. These precisely-measured and well-dated interglacial sequences provide evidence that little tectonic displacement has occurred since the late and middle Pleistocene.

3 Methods

The definition of paleo Relative Sea Level (RSL) from field proxies (here defined as RSL indicators) is related to the quantification of three main properties. These were first formalized by Shennan et al. (1982) and van de Plassche (1986) for Holocene sea level studies (see a recent review in Shennan et al., 2015 and applications in Khan et al., 2019), and

successively refined and adapted also to standardize RSL databases of older time periods (Rovere et al., 2016). In the simplest definition, each indicator used to reconstruct a paleo RSL should have three main characteristics: i) its elevation must be measured as precisely as possible and referred to a known tidal datum or a geoid model.; ii) it should be possible to quantify its indicative meaning (i.e. its relationship to the paleo sea level); iii) it should be possible to attribute an age to the facies indicating the paleo RSL. In this study, these three aspects were addressed as described below.

3.1 Elevation measurements

Elevations reported in this study were measured with a high-accuracy differential GPS (dGPS) receiving real-time Omnistar HP corrections (nominal 2σ or 95% accuracy of 0.1 m). In general, due to the presence of cliffs or other natural features masking the optimal satellite reception of the GPS signal, the average accuracy we obtained in the field is slightly lower than the nominal one: the measurement error associated with our points averages 0.6 m (2σ). All our elevation measurements were referred to the South Africa Geoid 2010 ("SAGEOID2010," Chandler and Merry, 2010). The discrepancy of this geoid with respect to mean sea level was estimated, in general, to be below 0.1 m. The measurement error associated with each RSL indicator was calculated as the square root of the sum of the squares of dGPS elevation measurement error and the geoid accuracy (0.1 m).

3.2 Quantification of the indicative meaning

Concerning the interpretation of RSL indicators, we subdivide them in different types (Table 1). To each indicator, we assign values of Reference Water Level (RWL) and Indicative Range (IR), that were calculated either from comparison with a modern analog (where available) or using the IMCalc tool (Lorscheid and Rovere, 2019). These values (RWL and IR) together compose the indicative meaning, and were used to calculate the elevation of the former RSL and the uncertainty associated with it (see formulations in Rovere et al., 2016). Landforms or deposits indicating a submerged environment or a terrestrial one, have been referred to as, respectively, marine or terrestrial limiting points (i.e., the sea level was respectively above, or below, the measured elevation of the landform or deposit). Because the approach of Lorscheid and Rovere (2019) assumes that both tidal ranges and wave properties in the past were similar to modern ones, we increased the final paleo RSL uncertainties of a further ±20% to account for possible deviations from this assumption.

3.3 Field research protocols

Each of the potential sites was initially reconnoitered to assess the quality of the exposures based on stratigraphic completeness and detail, abundance of potential sea-level related information, and presence of marine fossils for Sr dating. Once the optimal sections were identified, GPS and dGPS coordinates were taken. Key geomorphic, stratigraphic, and sedimentologic features, particularly major contacts and RSL indicators within the sections were photographed for broad and close up features. Our team of five marine geology specialists (with a combined century of experience) followed outcrops on foot, in the field for 100s of metres or longer in some cases, until the outcrop played out in all dimensions. While in the field, we observed, recorded, discussed and regularly challenged our own collective observations/interpretations of the outcrops. The key stratigraphic sections were vertically scaled to ±0.1 m using dGPS elevations. Key features (RSL indicators, contacts, sedimentary

facies transitions, etc. (e.g., Figure 4) were logged electronically, photographed, and recorded in field notes. Once documentation of the sections was achieved, samples of sediment and fossils were collected from identified stratigraphic units and saved in labeled and sealed plastic zip storage bags for future analyses.

Field sites and samples ID names all carry the preface "Z" for ZA (= RSA, Republic of South Africa). In the Northern Cape Province, near the village of Hondeklip, site and sample names are taken directly from those reported on quarry site maps provided by the De Beers Consolidated Mines. In other areas, "Z" prefixes two or three-letter abbreviations of nearby geographic place names from topographic maps, followed by numbered sections from within that area.

3.4 Chronological attribution and strontium isotope dating

In order to obtain accurate Sr isotope stratigraphy (SIS) ages of the shells collected from RSA paleo-shorelines, we applied a suite of criteria to assess the degree of post-depositional alteration of the shells. For the sample ages reported here, all chemical processing occurred at Lamont Doherty Earth Observatory (LDEO), and $^{87}Sr/^{86}Sr$ isotopes were measured using Thermal Ion Mass Spectrometry (TIMS) at SUNY Stonybrook.

Bivalve shells were initially screened based on visual inspection of shell thickness, the presence or absence of microborings and/or Fe and Mn staining (McArthur et al., 1994; del Rio et al., 2013). The most promising samples were fragmented, sonicated with quadruple distilled water, and then imaged using an optical microscope with CCD camera and an ASPEX Express scanning electron microscope (SEM). These images were assigned a preservation score ranging from "1" (no visible alteration) to "3" (significant alteration discernible) for each sample for both optical and SEM images, based on irregularities in crystal structure and above screening criteria (similar to Cochran et al., 2010). Minor and trace elements were also measured in duplicate for Sr, Mn, Mg, Al, Fe, and Ba on a Thermo iCap Q quadrupole ICP-MS at LDEO. High values of Mn, Mg, and Fe have been shown to be indicative of post-depositional alteration in marine carbonates (Shen et al., 1991; McArthur, 1994; Gothmann et al., 2015). We use these data to further eliminate samples that are likely influenced by diagenesis and recrystallization.

We used the "leach method" described by Bailey et al. (2000), which measures four or five sequential leachates on a single sample and which assumes that the more loosely bound diagenetic $^{87}Sr/^{86}Sr$ reservoirs will tend to be partitioned into the first leaches (Bailey et al., 2000; Li et al., 2011; Sandstrom et al., 2014). This advanced leaching protocol has the additional benefit of providing minimum or maximum SIS ages on the samples, based on trends within each leach set. If altering fluids are from a granitic source with high radiogenic $^{87}Sr/^{86}Sr$ ratios, SIS ages will be a minimum, as opposed to maximum ages if the sample is altered by a basaltic or older carbonate source with lower $^{87}Sr/^{86}Sr$ ratios. The trends in our sample leach sets always suggested a regional radiogenic (granitic) derived altering fluid, making SIS ages appear younger with more diagenesis (Sandstrom et al., 2014).

Sr was isolated and dried down using typical separation techniques with Eichon exchange resin and $^{87}Sr/^{86}Sr$ ratios were measured dynamically on an IsotopX Phoenix TIMS at Stonybrook University. The long-term instrument 2σ uncertainty determined by the Sr isotope standard NBS 987 (calculated annually over three years) varied between ± 0.0000126 (2014; n = 25) and ± 0.0000079 (2016; n = 40) (17-11 ppm, respectively). All Sr was

corrected for mass fractionation on the $^{86}Sr/^{88}Sr$ ratio of 0.1194 and adjusted by the NBS 987 standard value of 0.710248. After Sr isotope analyses of leaches, sample preservation was further evaluated from variation between $^{87}Sr/^{86}Sr$ measurements on each shell leach set (with smaller variation between initial and inner leaches generally associated with better preservation. SIS numerical ages were derived using the LOWESS Sr marine calibration curve from McArthur et al. (2012). Sample and terrace ages are based on averaging the better-preserved inner leaches (by filaments measured), age uncertainties are calculated using 2σ standard error of the mean. Only samples with an average preservation score less than "2" were used in terrace average.

4 Results

All our RSL data (including quantification of indicative meaning) and SIS ages are available in the PANGAEA repository as Hearty et al. (2019).

4.1 Study sites

The areas surveyed in this study are the western and southern coastlines of RSA (Figure 1). Overall, we surveyed the coastline between Hondeklip Bay in the Northern Cape Province to Groot Brak River near the town of Mossel Bay on the southern coast of the Western Cape Province. In the Northern Cape Province, at the mouth of the Olifants River, our surveys include an area called 'Avontuur' (same site as ZCP in this study, Roberts et al., 2011) (Figure 1C), that yielded several excellent natural cliff exposures and sections. Three areas were also surveyed along the Western Cape Province coastline between Cape Agulhas and Port Elizabeth, near Stilbaai (Figure 1F). The abundance of RSL indicators found at numerous sites (Table 2) identified in this study contrast markedly with the paucity of existing published data available from coastal Pliocene elsewhere in the world (Kaufman and Brigham-Grette, 1993; James et al., 2006; Raymo et al. 2011; Hearty et al., 2012; 2013; Rovere et al. 2014, 2015). In Table 3 and Figure 2, we present an overview of the samples that were dated using Sr isotopes. In the following paragraphs, we present the description of each RSL indicator and the rationale for our RSL interpretations.

4.2 Northern Cape Province – Hondeklip Bay

Along the Northern Cape Province (Figure 1B), during a cessation of operations at De Beers Consortium Mines, we visited a considerable number of exposures over several tens of kms in quarries and test pits. The exposures typically were cut through terrestrial colluvium and marine shoreface and foreshore deposits down to the bedrock abrasion platforms. Raw diamond deposits are excavated in gullies, moulins, and potholes in bedrock. In many cases, these sections expose the entire thickness of the marine formation in pits and quarry walls. This optimal setting allowed us to work on "clean" exposures (Figure 3D) devoid of vegetation, colluvium, slumping, and infrastructures that often obscure details and architecture of Quaternary and older shorelines.

ZSN29. Two stratigraphic sections were surveyed at this site. As in ZLKN_14.3 (see below), a distinct marine abrasion surface is carved in gneiss, forming the base of the section. Decimeter-scale cobbles with pebbles and sand (Figure 3H) on the abrasion surface are covered with articulated *in situ Ostrea* shells. The *Ostrea* themselves are further encrusted with the barnacles forming a sub-horizontal band surveyed up to +33.8±0.3 m (Figure 3I). A few tens of meters laterally within the same quarry pit, the cobble zone transitions to a sandy sedimentary environment exposing about 1.5 m thick, high-angle subtidal, cross-bedding

with abundant Ophiomorpha burrows (Figure 3J) and coarse pebble zones, reaching a maximum elevation of +32.8±0.5 m. A 0.5 m thick layer of concave-down (swash-oriented), and well-worn bivalve shells overlie the trough cross beds. The swash-oriented shells are buried by more than a metre of beach or eolian sand with terrestrial snail fossils (*Trigonephrus*?) and higher calcrete and *terra rossa* soil at +36 to +37 m, respectively. These sedimentary and biological RSL indicators combined are of the highest quality and indicative of a shallow marine environment.

ZSLT23. This site is exposed in an excavated trench test pit well above and landward of the several other investigated Hondeklip sites and thus represents the highest elevation fossiliferous marine site we studied in RSA. The base of the section contains largely disturbed/collapsed sandy sediment, presumably aeolian capped by a deeply reddened palaeosol about 0.3 m thick. Overlying is an imbricated boulder pavement with clasts ranging from 0.1 to >1.0 m and matrix of fossiliferous sand and gravel rises to +41.1±0.3 m (Table 2). A supratidal or transitional aeolian structureless sand 1-2 m thick and is capped by a reddish orange palaesol (0.3-0.5 m thick) and younger massive sands and brown soils. We interpret this facies as the uppermost reaches of the beach and/or storm deposit, therefore a terrestrial limiting (i.e., this section, at the time of formation was probably above Mean Higher High Water). An abraded and highly altered *Ostrea* shell from this deposit was measured using the leach method, and showed older SIS ages with each leach, indicative of highly radiogenic $^{87}Sr/^{86}Sr$ alteration fluids. From this leach trend and degree of weathering we can only assign a strict minimum SIS age of 2.23 Ma to the terrace with a large uncertainty (2.23 to 4.19 Ma) due to analytical uncertainty and diagenetic alteration of the shell sample (Table 3); the actual terrace age is probably significantly older than 2.23 Ma based on morphostratigraphic context.

ZLK_N3. A succession of high-angle subtidal trough cross beds transitioning to planar beach beds is exposed at ZLK_N3. This transition represents the most accurate paleo RSL indicator in this section measured at +30±0.2 m (Figure 3A). This shallowing-upward sequence is truncated and incised by a small runnel or gully filled with highly abraded, concave downward bivalve shells characteristic of a wave swash environment (Figure 3B). Both subtidal and intertidal beds contain oyster and bivalve mollusk shells.

ZLK_N6. Two sections, North and South, were logged at this location. The base of the South section exposes an assemblage of multiple storm (?) beds containing coarse abraded shelly material with numerous disoriented valves of the oyster *Ostrea* and abundant whale bones (Figure 3C). There are no precise RSL indicators in these two sections. Although it could represent an upper-shoreface or near-foreshore environment (with whale bones resulting, for example, from strandings in shallow water or on the beach), we opt to characterize this site as a marine limiting. As elevation of this site, we use that of a sharp erosional contact between subtidal marine beds and terrestrial deposits at +14.8±0.3 m. A similar complex succession 50 m from the South section occurs at North section with subtidal trough cross beds and *Ophiomorpha* burrows. Within the subtidal beds, an *Ostrea* valve measuring over 55 cm long (Figure 3C) was observed. The subtidal unit is overlain by a series of alternating sandy and coarse storm beds (possibly deposited on the shelf) similar/equivalent to the adjacent southern site. At a sharp erosional contact, subtidal cosets are truncated by terrestrial deposits at +12.6±0.2 m.

ZLKN_14.3. At this site, a wave abrasion surface on gneissic bedrock (Figure 3D) is mantled by a sub-metre-scale boulder pavement with abundant attached oysters (Figure 3F). A sub-

horizontal band of barnacles can be traced continuously along the boulder deposit (Figure 3E) at +28.8±0.4 m. About 1 m of structureless beach sand above the boulders grades upward into terrigenous deposits and a palaeosol. The lack of sedimentary structures in this sandy unit may be the result of bioturbation by nearshore and land organisms. This geomorphological and palaeo environmental setting of this site is analogous to modern intertidal shore platform and boulder fields in the adjacent modern shoreline, where we measured a modern band of barnacles at +0.8 m, slightly below the high tide mark measured at +1.8 m on the same modern shoreline (Figure 3G).

4.3 Northern Cape Province - Olifants River mouth

ZCP1/2. The ZCP site (Figure 4) at Cliff Point is located north of the Olifants river mouth (Figure 1C). Based on similar elevation and stratigraphic components, we correlate Cliff Point with sites surveyed in the Northern Cape Province (e.g., ZLK_N14.3; ZSN29) near Hondeklip. We measured a distinct wave abrasion platform carved in the bedrock, composed by Neoproterozoic Gariep Supergroup metasediments (Pether et al., 2000; Roberts et al., 2011), gently sloping towards the sea. The modern abrasion platform is shown in Figure 5A. The highest measurable point on the platform is +29.1±0.3 m (Figure 5A, B and Figure 4). The platform surface is mantled with reworked pebbles and boulders up to 1 m in diameter, many encrusted on their upper surfaces by marine calcareous algae and serpulid tubes (Figure 5D). The boulder beds are overlain by a 5-6-m thick, shallowing-upward foreshore sedimentary sequence. Nearby, we surveyed a weakly-bedded subtidal unit, composed of coarse sands and gravels, 2-2.5 m higher than the platform surface, which is then succeeded by prominent high-angle trough cross beds. Above a sharp transition at +33.9±0.3 m (Figure 5C), the intertidal beds are capped by a coarse cobble and shell-rich bed about 1.5 to 2.0 m thick, interpreted as the swash zone. The highest capping shell bed, rising to near +38 m as backshore supratidal facies, is composed almost entirely of *Donax rogersi or D. haughtoni*, many of which are articulated, but chaotically distributed and disoriented in a terrigenous sandy matrix, unlike their living habitat in the lower surf zone. However, the field interpretation of the marine and supratidal facies appears to have caused some of the discrepancy between highstand elevations. Our dGPS elevation of the abrasion platform differs from Roberts' et al.'s (2011) "Avontuur" (same site) measure by less than a meter (+30 m vs +29.1 m), and we interpreted that the highest *storm* deposits marking the highest reach of the sea is about +38 m, in agreement with Roberts' measurements. Nonetheless, we interpret the sharp shoreface-foreshore facies transition at +33.9 m (Figure 4) as the best RSL indicator in the sequence. The SIS age from the best preserved *Ostrea* shell at this deposit yielded an age of 4.63 ± 0.36 Ma (Table 3, Figure 2). This sample had a shallow downward sloping Sr leach trend (less than 6 ppmv $^{87}Sr/^{86}Sr$ isotope variation across the first to last leach) indicating good preservation despite relatively elevated imagery and elemental scores. This shallow dipping leach trend is consistent with a radiogenic $^{87}Sr/^{86}Sr$ regional alteration fluid, causing sample SIS ages to appear younger with diagenesis.

ZCH1/2. The sites we surveyed at ZCH, Channel Site, are stratigraphically complex and more challenging to interpret. However, some important sea-level data can be derived from two neighboring sections. At ZCH1, a horizontal marine abrasion platform (with borings of marine organisms) is formed in altered gneiss at circa +14 m and blanketed with a coarse cobble and pebble zone about 20-30 cm think (Figure 5E). The alternating sand and pebble zones above are interrupted by more indurated lenses of finer sand. Subtidal trough cross beds rise to +15.0±0.3 m and, together with the abrasion platform at +14 m, show that a former RSL was close to this elevation. At this site, a 1.5 m thick bed of *D. rogersi* in a

coarse pebble-sand matrix is exposed above a second sharp erosional contact. The shells are roughly oriented concave down in the lower part, but *chaotically distributed* in the upper few decimeters, up to +16.1±0.3 m. Most of the lower part of the section ZCH2 exposed in a nearby gully is covered except for the upper part subtidal beds that are similar to ZCH1. The chaotic bedding with *D. rogersi* is repeated up to +18.6±0.5 m where it is capped by terrestrial colluvium.

ZDG1-4. At Donkergat, four adjacent sections (ZDG1-4) can be represented as a composite. A marine abrasion platform at +14±0.4 m, carved into reddish Palaeozoic sandstones, is mantled by large (some >1 m) boulders, cobbles in a coarse matrix of shelly sands (Figure 5F, G). (At the inner margin of the active marine abrasion platform adjacent to this section, we measured the platform at +1.4 m). Numerous bivalves in this marine sand, including *D. rogersi* at +15.5 m are articulated indicating shallow subtidal conditions. Small alternating lenses of indurated finer sand and coarser layers with surf-oriented bivalves rise up to +18.7 m. Above the densely-packed intertidal, oriented shells in beach beds, lies a deeply reddened sand with abundant rhizomorphs and fossil termite mounds, and 0.5 to 1.0 m thick beds of chaotically bedded and containing numerous articulated valves of *D. rogersi* rising to +19.3 m (Figure 5H). As in other cases, we consider these beds to be the product of a severe storm or tsunami that ripped up the shallow subtidal and beach environment, transporting the living surf clams well up into the supratidal zone; soon thereafter being recolonized by termites and land plants. Two bivalves (a *Donax* and *Dosinia sp*.) were dated from this deposit and both passed our screening tests. The average SIS age from those two shells (6 measurements) is 1.04 ± 0.16 Ma (Table 3, Figure 2). This terrace age thus corresponds with the mid-Pleistocene and overlapping within uncertainty to the interglacial MIS 31, which has been shown to be an exceptionally warm period (de Wet et al., 2016).

4.4 Western Cape Province - West Central coast

ZPPH. An informative shallowing-upward shoreline succession is observed in an active quarry at ZPPH (Prospect Hill), near the city of Saldanha (Figure 1D). At the base of the quarry exposure, a large granite boulder (~1.5 m diameter) is surrounded by high concentrations (compared to other parts of the exposure) of *Patella/Fissurella* (many *in situ* cemented on the boulder surface) and rock grazing gastropods (Figure 6A,B). This boulder in a shallow subtidal environment would function as a breakwater, “attracting” coarser sediments and shells, as well as the limpets attached to the granite higher in an intertidal zone. In a 3-4 m-thick sequence, subtidal trough cross beds around the boulder transition to pebbly planar beach beds at +11.5±0.5 m and upward into a structureless (bioturbated), pedogenic sand with abundant pulmonate gastropods (*Trigonephrus globulus*). A second, higher aeolianite several meters thick, on a reddish weathering surface, contains large festoon cross-bedding and the same land snails at the upper surface.

4.5 Western Cape Province - South coast

ZDH. In the region near De Hoop Nature Preserve, a broad marine terrace at +25-33 m extends several tens of kilometers inland from near the modern coastline (Figure 7A). At its seaward edge, the terrace is mantled by a relatively thin ‘caprock’ measured at +26.3 ±1 m, composed of fossiliferous marine calcareous grainstone and biorudstone (Figure 7B) with occasional large preserved shells including abundant, ~10 cm size, concave-down oriented *Glycymeris* (Figure 7C), indicating a swash zone depositional environment. With no other sedimentologic constraints, we interpret this deposit as forming from the Storm Wave Swash Height to the depth of breaking of modern significant waves in this area. Using as RSL

indicator the elevation of the inner margin of the large marine terrace (+28.3 ±1.0 m), Rovere et al. (2014) calculated that this site represents a paleo-RSL at +29.8 ±1.8 m, which we recalculate in this study (with a slightly different interpretation of the indicative range) to +26.3 ±4.2 m (Table 2).

ZBR1. Along the open terrace plain south of Bredasdorp (located 50 km southwestward on the same marine terrace plain as ZDH, Figure 7D), we discovered a moderately indurated marine surface at +21.9 ±0.2 m near the roadside. However, unlike De Hoop, the shells of ZBR1 were in a matrix of fine marl and in variable in orientation, with many valves articulated in living position (Figure 7E). The random orientation of the shells and occasional articulation would likely be the result of active bioturbation on a living shallow sea floor. Rovere et al. (2014) interpreted this facies as marine limiting. We note that the same study interpreted the inner margin of the scarp at ZBR1 representing paleo SL elevations at+24.02±1.51 m, while here we rely only on the stratigraphy of the site to interpret the sea level information. In fact, we interpret the roadside outcrop to indicate a deeper offshore subtidal marine sand/marl with fossils deposited in water depths generally below wave base. This interpretation better reconciles RSL at this site with that derived from the nearby site ZDH. A *Glycymeris* shell from ZBR1 produced a highly robust SIS age of 3.10 ± 0.29 Ma, while an *Ostrea* shell from the same deposit recorded a SIS age of 2.95 ± 0.43 Ma (Table 3, Figure 2). Variation between the leach sets are 1.1 and 3.6 ppm, respectively, demonstrating excellent preservation. The average SIS age of the terrace based on these two shells (10 measurements) is 3.01 ± 0.40 Ma (Table 3, Figure 2). A large part of this uncertainty is based on the shallow slope of the SIS curve over this time period, as the actual $^{87}Sr/^{86}Sr$ leach measurements show little variation (Table 3).

ZST1 to 3. Three areas were surveyed along the southern coastline between Cape Agulhas and Port Elizabeth. Near Stilbaai, steep and vegetated outcrops in three separate road cuttings yielded limited datable shell material, but at these sites we could document wave abrasion surfaces in weathered and unstable bedrock of deformed Palaeozoic shale averaging at +17.8±0.4 m, +15.8±0.5 m, and +22.3±4.1 m (the larger error range at this latter site is due to a poor GPS precision at the time of measurement). On some of these terraces, we sampled small samples of weathered shell hash deposited amongst a coarse cobble bed generally less than 0.5 m thick. Unstructured marine sand and silt 1-3 m thick cap the exposed sections.

5 Discussion

5.1 Plio-Pleistocene RSL indicators in South Africa

Over the last decade, there has been a growing inventory of preserved field proxies related to Pliocene sea-level highstands (Raymo et al., 2011; Rovere et al., 2014, 2015; Dumitru et al., 2019; Grant et al., 2019). The arid western and southern coasts of RSA offer nearly ideal conditions for the formation and preservation of fossil coastal deposits. Here, we document numerous Pliocene and Pleistocene sites (Table 2 and 3). The large number of RSL indicators we surveyed confirms previously published observations of *at least* two major terraces of different ages between +32 and +17 m along the Northern and Western Cape Provinces, in general agreement with the classic study of Carrington and Kensley (1969) and, more recently, Roberts et al. (2011).

Some of the sites reported here (e.g., ZLK_N_14.3 and ZSN29) have preserved very precise fixed biological RSL indicators that constrain former RSL positions with sub-meter accuracy.

Dumitru et al. (2019) document similar precision from the physical phreatic overgrowth of Pliocene speleothems in Mallorca (Spain, NW Mediterranean Sea), yet sea-level estimates involve large background uncertainties (~68%) when isostatic adjustment, dynamic topography and uplift rates especially in an active tectonic plate zone as in the Mediterranean. While most RSL indicators we report are of high-quality and precisely measured, we also recognize that there might be factors affecting our quantification of the indicative meaning. In fact, the precision of almost all our indicative meaning estimates depend, ultimately, on measured or modelled tidal or wave data. In order to account for this possible bias, we added a further uncertainty of 20% to our field data. Of note is that there are active debates on whether paleo waves (for MIS 5e, see Hansen et al., 2016; Rovere et al., 2017, 2018; Hearty and Tormey, 2017; 2018) were stronger than modern ones. Also, tidal ranges are naturally subject to greater or lesser amplitudes when sea levels change (Hill, 2016; Lorscheid et al., 2017; Wilmes et al., 2017). The quantification of such changes with hydrodynamic models is, to some extent, possible within the Holocene, where shelf bathymetric changes are relatively well constrained (e.g., Hill et al., 2011) and where high-resolution, fine sedimentary successions are available (e.g., Roep and Beets, 1988). Expanding the concepts already employed for Holocene and Pleistocene tidal and wave energy changes also to older periods is surely a promising avenue for future research.

We also remark that, among our sites, only two (ZCP Section 2 and ZDG) qualify as valid RSL indicators following the definition of Shennan et al. (1982) and van de Plassche (1986), mostly due to dating constraints. In fact, finding and identifying well-preserved samples for Sr isotope dating is always a challenge with Plio-Pleistocene aged carbonate shorelines. There is also an unavoidable error of 0.11 to 0.47 Ma for $^{87}Sr/^{86}Sr$ dating of fossil materials due to the flatness of the Sr-isotope curve during the Pliocene period (McArthur and Howarth, 2012). Micro-sampling combined with a range of preservation screening protocols (this study) within single organisms adds needed confidence to the robustness of SIS age estimates. A third site dated with SIS is ZBR (elevation +21.9 ±0.2 m), that is interpreted in this study as marine limiting, i.e., deposited below Mean Lower Low Water. Correlating ZBR with ZDH, located 50 km to the East and resting upon the same extensive terrace (Rovere et al., 2014), it is possible to assign the ZBR age to the paleo RSL at ZDH (+26.3 ±4.2 m), as shown in Figure 8B.

In addition to the RSL information we provide in this paper, we note that a few sites contain chaotic deposits, mainly containing the surf clam *Donax*, often articulated but generally set in rubified, terrigenous sands often among fossil termite mounds (Figure 5H). These deposits (ZCP1, ZCH1/2; ZDG1) have elevations ranging from +38 to +18 m, and we propose they are most likely the result of rapid sea-level shifts, intense storms or tsunami events.

5.2 Topographic Zones

Based on our research, we describe three main topographic zones in which a number of sites from our study occur. These arbitrary zones do not necessarily define isolated sea-level events, but reflect simply the *topographic zones by elevation* in which different sites occur. We refer to the zones from highest elevation to the lowest as Zone I (+25-35 m), Zone II (+15-20 m), and Zone III (that we attribute to mid to late Pleistocene; <14 m). The RSL indicators we measured in RSA and the correlated ages and paleo RSL interpretations are summarized in Figure 8.

Topographic Zone I (+25-35 m). This zone includes sites ZSN 29, ZLK_N14.3, ZLK_N3, ZCP and ZDH (Figure 8A), and appears to be distributed along the Northern and Western Cape Provinces. One section at ZCP (Cliffs Point) yielded a Sr age of 4.63 Ma (Max 4.87, Min 4.28 Ma), which appears to closely correspond with the mid Pliocene Climatic Optimum (4.0-4.4 Ma, Figure 8B). A broad terrace along the Southern coast includes both DeHoop (ZDH) and Bredasdorp (ZBR) sites, which yielded marine facies from two sites between +28 to >+22 m; the latter associated with a Sr age of 3.01 Ma (Max 3.40 Min 2.73 Ma). Another site, in the Northern Cape Province (ZSLT23), yielded only a minimum age (older than 2.23 Ma) and represents a terrestrial limiting point, but is in agreement with the overall characterization of Zone I with early and late Pliocene events.

Topographic Zone I appears to correlate with a broad terrace 850 km north of our northernmost site (ZSN29), in Namibia. There, Stollhofen et al., 2014 report a marine terrace level at +33.8 m. However, these authors invoked a tectonic element to explain this high sea-level position. Along the Roe Plains of southwestern Western Australia, James et al. (2006) described the nature of the Pliocene Roe deposits and estimated the maximum sea-level position at +30 m. In the southeastern USA, Rovere et al. (2015) tracked and documented the dGPS elevation the Pliocene (MPWP?) "Orangeburg Scarp" and equivalents from Georgia to Virginia (Dowsett and Cronin, 1990). Indeed, the geomorphic sea-cliff scarp measured elevations of ~37 m in Georgia, ~60-80 m in South and North Carolina, and ~80 m in central Virginia (Rovere et al., 2015). As we anticipated, the Pliocene of the southeast USA highlights a more extreme example of post-depositional effects (±20 m on same scarp), particularly GIA and DT attributed to the proximity of ice sheets and other tectonic effects.

Topographic Zone II (+15-20 m). In both Northern and Western Cape Provinces, RSL indicators were also measured at several sites around 15-20 m (Figure 8A). One site, ZDG, is associated with a Sr age of 1.04 Ma (Max 1.18, Min 0.88 Ma). In the same area, 10 km from this site, ZCH1/2 can be also attributed to Topographic Zone 2. The two sites measured at Still Baai (ZST, Figure 8A), may be correlated with ZDG, but caution is advised in such correlation as there are more than 540 km of coastline separating ZDG and ZST. In any case, Topographic Zone II would yield an apparent correlation with MIS 31, that is usually dated at 1.08-1.06 Ma (Lisiecki and Raymo, 2005).

Topographic Zone III (<15m). Zone III incorporates later Pleistocene sites reported in literature (Carr et al., 2010, Roberts et al., 2012), with MIS 11 and MIS 5e coastal deposits found along the coastlines we surveyed at, respectively, +13-14 m and +4 to +8 m.

5.3 The Pliocene sea level "buzz saw"

Pliocene shorelines were constructed under obliquity-dominated (41 kyrs) sea-level regime (Lisiecki and Raymo 2005). Naish et al. (2009) showed that high-frequency, low-amplitude SL oscillations of ca. ~13 m over glacial-interglacial cycles persisted between 3.3 and 2.5 Ma (Grant et al., 2019). It is likely that oscillations of similar magnitude persisted throughout most of the Pliocene, for a duration of perhaps 3 million years. This resulted in the formation of vast, broad terraces tens of km wide, and in some cases, hundreds of km long (James et al., 2006; Kendrick et al., 1991). Examples such features are the De Hoop coastal plain (Figure 7A), and similar coastal features in Western Australia and the US East Coast (Rovere et al., 2014, 2015).

Hearty et al. (2012; 2016) characterized this process of terrace cutting as a sea level "buzz saw." In morphological contrast, eccentricity-dominated (100 kyrs) mid to late Pleistocene highstand events (high amplitude, low frequency) for the past 500 ka incised much narrower terraces and benches over typically short, 10-15 ka highstand intervals. Given the sheer morphological scale of 10s to 100s of km of Plio-Pleistocene terraces and deposits around the world it is postulated that the highstand events that we have identified are among some of the higher and later of the potentially large numbers of highstand deposits that occurred in this broad topographic zone. Erosional processes likely to have occurred would include repeated transgressions, reoccupation of fledgling terraces, erosion and removal of older terrace sediments, and their replacement with contemporaneous deposits.

The Pliocene sea level "buzz saw" may appear to be at odds with the terrace erosion modeling results of Trenhaile (2014), who conclude that "*The large oscillations of the middle to late Quaternary were more conducive to erosion than the smaller oscillations of the Pliocene and early Quaternary…"* Volumetrically, the large sea-level oscillations of the later Pleistocene may indeed have eroded more material; however, in terms of geomorphic expression, the Pliocene buzz saw processes certainly created the larger and more impressive landforms by comparison. We highlight that, in this regard, our study area and the results we present in this study may represent an ideal benchmark to test different erosion model parameters.

5.4 Long-term vertical land motions

The high-resolution data we report in this study represent RSL estimates: this means that they are still uncorrected from any quantifiable departure from eustasy that might have affected their elevation since they were deposited. Even considering tectonics as negligible, we cannot directly discount potentially relevant effects of DT in our study areas. Rovere et al. (2014) highlight that, even at passive margins and with highly precise RSL indicators, the large uncertainty in DT models make assumptions on the eustatic sea level more challenging in the Mid Pliocene Warm Period (ca. 3 Ma).

We find a striking match between one of our dated records (ZCP Section 2, SIS age=4.28-4.87 Ma) and the oldest phreatic overgrowth on the Mallorca speleothems recently reported by Dumitru et al. (2019) (AR-02, U-Pb age=4.39±0.39 Ma, 2σ). With a full account, and given uncertainties related to post-depositional displacement of the Mallorcan site, Dumitru et al. (2019) calculated that the global mean sea level at this time (without correction for thermal expansion) was between +10.6 and +28.3 m above present (16th and 84th percentiles uncertainty bounds). For the sake of discussion, we offer this assumption: the predicted GIA reported by Rovere et al. (2014) for the Mid-Pliocene Warm Period (ca. 3 Ma, 3.6±1.2 m) is not significantly different from GIA at the time of ZCP formation. Using these values of eustatic sea level, GIA and RSL obtained at ZCP (35.1±2.2 m), we calculate that a first-order estimate of long-term post-depositional vertical land movements in the area of interest is in the order of 2.6 m/Ma (50^{th} percentile, with 33^{rd}-66^{th} percentile bounds 2.0 – 3.3 m/Ma, see Rovere (2020) for methods). We note that rate is slightly lower than the one proposed by Rudge et al. (2015) over the last 13±5 Ma for Hondeklip Bay (ca. 160 km to the North, 8±3 m/Ma) and one order of magnitude lower than the uplift rate calculated by the same authors for Saldanha Bay (ca. 160 km to the South, 20±10 m/Ma).

Our calculation implies that, while numerical models of DT in our study area are discrepant (e.g., see Moucha et al., 2008; Spasojevic and Gurnis, 2012; Austermann et al., 2017), there

is evidence only for limited uplift, in the range of few meters per million years. The rate calculated here would affect only minimally MIS 5e and MIS 11 (overall, less than 1.5 m). The MPWP, dated at ZBR (and correlated with ZDH RSL reconstructed at +26.3±4.2 m, Figure 8B), would have been displaced by 6 to 10 meters and the MIS 31 RSL we dated at ZDG (RSL=14.2±2) would have been displaced by only 2-3 meters.

6 Conclusion

In this study, we reported RSL indicators from the Northern and Western Cape provinces in South Africa. While only three of seventeen surveyed sites yield reliable ages (plus one minimum age), these are among the few well-dated, precisely measured and interpreted RSL indicators for the Pliocene and Early Pleistocene. In fact, we document that paleo RSL imprints were left along these shorelines at two prominent topographic zones, at +25-35 m and +15-20 m. The highest (Zone I) appears correlated to multiple Pliocene sea levels (ca. 3-5 Ma), while the second (Zone II) with a peak sea level during the early Pleistocene (ca. 1 Ma, possibly coinciding with MIS 31). A third topographic zone (Zone III, below +14 m) has conserved the imprints of late Pleistocene sea level changes (MIS 5e and MIS 11, as reported in Carr et al., 2010 and Roberts et al., 2012).

In the Western Cape Province the morphology of the broad terrace associated with Zone I matches similar landforms at different sites (e.g. US East Coast, or Australia, Rovere et al., 2014). Here, we define this as a sea level erosional terrace, that was produced by repeated small-amplitude sea-level oscillations (Grant et al., 2019). The results of this study represent an ideal real-world benchmark as the science on long-term landscape erosion models progresses (De Gelder, 2020).

The Plio-Pleistocene paleo RSL estimates presented here represent a robust dataset against which future studies of long-term tectonic uplift or global mean sea level can be based. The overlap between our oldest RSL indicator (ZCP) and the oldest RSL indicator reported by Dumitru et al. (2019) (both with average ages between 4.4 and 4.6 Ma) allowed us to speculate on the possible long-term vertical land motions in our study area, which would be relatively low (2 – 3.3 m/Ma). While caution should also be adopted in propagating long-term rates linearly through time (Stocchi et al., 2018), propagating these rates onto the two younger shorelines dated in this study (3 ma and 1 Ma, ZBR/ZDH and ZDG, Figure 8B) sustains the recent results by Grant et al. (2019), who limited the upper bound of Pliocene sea level rise to less than +25 m. The same calculations indicate that MIS 31 may have peaked at a similar elevation to MIS 11 (+9-14 m, Raymo and Mitrovica, 2012).

The glaciological implications of this study are significant. The *minimum* sea-level elevations of Zone I of ca. +27 m (that would be only marginally affected by DT under our assumptions) implies that melting of Greenland, West Antarctica, and marine-based ice sheets of East Antarctica (about a third of all polar ice) occurred during a Pliocene 400 ppmv world. Confirmation of significantly higher sea-level elevations would involve the retreat of additional land-based Antarctica ice. During the middle Pleistocene, sea level also rose to +9 to +17 m in both MIS 11 and 31, despite the fact that CO_2 concentrations probably did not exceed 300 ppmv. Our study confirms that ice sheets are highly vulnerable under warming climates, and are likely to experience dynamic changes when subject to climatic parameters of today and those predicted for decades and centuries to come.

Acknowledgments, Samples and Data

Dr. David Lester Roberts (Dave) was instrumental in unraveling the late Cenozoic natural history of South Africa (and elsewhere) over the past decades. He made significant discoveries in ancient rock record, palaeoclimate, SL, megafauna, human footprints and origins in South Africa, Gabon, and Madagascar. Our collaboration with Dave in the field was friendly and adventuresome but safe, inspiring and highly informative, thanks to his extensive knowledge of the region. His contributions were instrumental in the major findings of this paper. We were truly saddened to learn of his untimely death in 2015.

This research investigation was among the primary objectives of the "PLIOMAX" grant NSF OCE-1202632 (PI MER and co-PI PJH). MER also appreciates support from the Vetlesen Foundation. The authors acknowledge PALSEA (a PAGES / INQUA) working group for useful discussions and comments at the 2012 meeting (Rome). Council of Geosciences RSA provided full logistic and field support for coauthor D Roberts. The authors also thank E Bergh (Natural History Department Iziko South African Museum) for his dedicated work in the field and Iziko Museum in Cape Town for providing important materials. De Beers Consolidated Mines provided access, vehicle, and a guide, and allowed several days of examination and collection of the quarries and test pits. Mr. Justin Gillis joined our expedition to tell our story to The New York Times (https://www.nytimes.com/2013/01/22/science/earth/seeking-clues-about-sea-level-from-fossil-beaches.html). This research was conducted in the Republic of South Africa under SAHRA Permits (Ref. 80/12/06/001/61, 9/2/066/0001). The background maps in Figure 1 of this article were created using ArcGIS® software by Esri. ArcGIS® and ArcMap™ are the intellectual property of Esri and are used herein under license. Copyright© Esri. All rights reserved. For more information about Esri® software, please visit www.esri.com. We appreciate the informative and constructive reviews (and re-review) provided by T. Naish, T. Törnqvist, and an anonymous reviewer that greatly improved this manuscript.

Data and samples availability. Data for this research are available below in Supporting Information and in PANGEA at this DOI: (https://doi.pangaea.de/10.1594/PANGAEA.910120) under a Creative Commons Attribution 4.0 International license. All our samples are registered with an IGSN in SESAR (http://www.geosamples.org/igsnabout)

References

Austermann, J., Mitrovica, J.X., Huybers, P., & Rovere, A. (2017). Detection of a dynamic topography signal in last interglacial sea-level records. *Science Advances,* 3:e1700457. doi: 10.1126/sciadv

Baby, G., Guillocheau, F., Braun, J., Robin, C. and Dall'Asta, M. (2020). Solid sedimentation rates history of the Southern African continental margins: Implications for the uplift history of the South African Plateau. *Terra Nova*, 32(1), pp.53-65.

Bailey, T. R., McArthur, J. M., Prince, H., & Thirlwall, M. (2000). Dissolution methods for strontium isotope stratigraphy: whole rock analysis. *Chemical Geology,* 167, 313-319.

Carr, A.S., Bateman, M.D., Roberts, D.L., Murray-Wallace, C.V., Jacobs, Z., & Holmes, P.J. (2010). The last interglacial sea-level high stand on the southern Cape coastline of South Africa. *Quaternary Research*, 73, 351–363.

Carrington, A.J. & Kensley, B. F. (1969). Pleistocene molluscs from the Namaqualand coast. *Annals of the South African Museum*, 52, 189-223.

Chen, F., S. Friedman, C.G., Gertler, J., Looney, N. O'Connell, K. Sierks, and J.X. Mitrovica. (2014). Refining Estimates of Polar Ice Volumes during the MIS11 Interglacial Using Sea Level Records from South Africa. *Journal of Climate*, 27, 8740–8746, https://doi.org/10.1175/JCLI-D-14-00282.1

Chandler, G., Merry, C.L., 2010. The South African Geoid 2010: SAGEOID10, PositionIT.

Cochran, J. K., Kallenberg, K., Landman, N. H., Harries, P. J., Weinreb, D., Turekian, K. K., et al. (2010). Effect of diagenesis on the Sr, O, and C isotope composition of late Cretaceous mollusks from the Western Interior Seaway of North America. *American Journal of Science*, 310(2), 69–88. http://doi.org/10.2475/02.2010.01

Dale, D.C., McMillan, I.K., 1999. On the Beach. Field Guide to the Late Cainozoic Micropaelontological History of the Saldanha Region, South Africa. 127 pp.

Dauteuil O., Bessin P., and Guillocheau F. (2015). Topographic growth around the Orange River valley, southern Africa: a Cenozoic record of crustal deformation and climatic change. *Geomorphology*, 233, 5-19.

DeConto, R. M. & Pollard, D. (2016). Contribution of Antarctica to past and future sea-level rise. *Nature*, 531, 591–597.

de Gelder, G., Jara-Muñoz, J., Melnick, D., Fernández-Blanco, D., Rouby, H., Pedoja, K., Husson, L., Armijo, R. and Lacassin, R., 2020. How do sea-level curves influence modeled marine terrace sequences? *Quaternary Science Reviews*, 229, p.106132.

del Río, C. J., Griffin, M., McArthur, J. M., Martínez, S., & Thirlwall, M.F. (2013). Evidence for early Pliocene and late Miocene transgressions in southern Patagonia (Argentina): 87Sr/86Sr ages of the pectinid "Chlamys" actinodes (Sowerby). *Journal of South American Earth Sciences*, 47(C), 220-229. http://doi.org/10.1016/j.jsames.2013.08.004

de Wet, G.A., Castañeda, I.S., DeConto, R.M., & Brigham-Grette, J. (2016). A high-resolution mid-Pleistocene temperature record from Arctic Lake El'gygytgyn: a 50 kyr super interglacial from MIS 33 to MIS 31?: *Earth and Planetary Science Letters*, v. 436, p. 56-63. http://dx.doi.org/10.1016/j.epsl.2015.12.021.

Dowsett, H.J., & Cronin, T.M., (1990). High eustatic sea level during the middle Pliocene: Evidence from the southeastern US Atlantic Coastal Plain. *Geology*, 18, 435–438.

Dumitru, O.A., Austermann, J., Polyak, V.J., Fornós, J.J., Asmerom, Y., Ginés, J., Ginés, A. & Onac, B.P. (2019). Constraints on global mean sea level during Pliocene warmth. *Nature*, 574, pp.233-236.

Dutton, A., Carlson, A.E.E., Long, A.J.J., Milne, G.A.A., Clark, P.U.U., DeConto, R., Horton, B.P., Rahmstorf, S., & Raymo, M.E., (2015). Sea-level rise due to polar ice-sheet mass loss during past warm periods. *Science*, 80-.349, aaa4019-aaa4019. doi:10.1126/science.aaa4019

Egbert, G.D., Bennett, A.F., & Foreman, M.G.G. (1994). TOPEX/POSEIDON tides estimated using a global inverse model. *Journal of Geophysical Research*, 99. doi:10.1029/94JC01894

Egbert, G.D., & Erofeeva, S.Y. (2002). Efficient Inverse Modeling of Barotropic Ocean Tides. *Journal of Atmosphere and Ocean Technology*, 19, 183–204. doi:10.1175/15200426(2002)019<0183:EIMOBO>2.0.CO;2

Fischer, H., Meissner, K.J., Mix, A.C. Abram, N.J., Austerman, J., Brovkin, V. et al. (2018). Palaeoclimate constraints on the impact of 2°C anthropogenic warming and beyond. *Nature Geoscience*, 11, 474-485. doi.org/10.1038/s41561-018-0146-0.

Forstén, A., (1992). Mitochondrial DNA time-table and the evolution of *Equus*: comparison of molecular and paleontological evidence. *Annales Zoologici Fennici*, 28: 301-309.

Golledge, N.R., Keller, E.D., Gomez, N., Naughten, K.A., Bernales, J., Trusel, L.D., & Edwards, T.L., (2019). Global environmental consequences of twenty-first-century ice-sheet melt. *Nature* 566, 65-72. doi.org/10.1038/s41586-019-0889-9.

Gothmann, A. M., Stolarski, J., Adkins, J. F., Schoene, B., Dennis, K. J., Schrag, D. P., et al. (2015). Fossil corals as an archive of secular variations in seawater chemistry since the Mesozoic. *Geochimica Et Cosmochimica Acta*, 160(C), 188–208. doi:10.1016/j.gca.2015.03.018.

Grant, G. R., Naish, T. R., Dunbar, G. B., Stocchi, P., Kominz, M. A., Kamp, P. J. J., Tapia, C. A., McKay, R. M., Levy, R. H., & Patterson, M. O. (2019). The amplitude and origin of sea-level variability during the Pliocene epoch. *Nature Geoscience*, 1476-4687. https://doi.org/10.1038/s41586-019-1619-z, 10.1038/s41586-019-1619-z

Hansen, J., Sato, M., Hearty, P., Ruedy, R., Kelley, M., Masson-Delmotte, V., *et al.* (2016). Ice melt, sea level rise and superstorms: Evidence from paleoclimate data, climate modeling, and modern observations that 2°C global warming could be dangerous. *Atmospheric Chemistry and Physics*, 16, 3761–3812. doi:10.5194/acp-16-3761-2016

Haughton, S.H. (1931). The Late Tertiary and Recent deposits of the West Coast of South Africa. *Transations of the Geological Society of South Africa*, 34, 19–58.

Hearty, P.J. & Tormey, B.R. (2017). Sea-level change and superstorms; geologic evidence from the last interglacial (MIS 5e) in the Bahamas and Bermuda offers ominous prospects for a warming Earth. *Marine Geology*, 390, 347-365. doi.org/10.1016/j.margeo.2017.05.009

Hearty, P.J., & Tormey, B.R. (2018). Listen to the whisper of the rocks, telling their ancient story. *Proceedings of the National Academy of Science*, 10.1073/pnas.1721253115.

Hearty, P.J., Kindler, P., Cheng, H., & Edwards, R.L. (1999). A+20 m middle Pleistocene sea-level highstand (Bermuda and the Bahamas) due to partial collapse of Antarctic ice. *Geology* 27, 375-378.

Hearty, P.J., Hollin, J.T., Neumann, A.C., O'Leary, M.J., & McCulloch, M. (2007). Global sea-level fluctuations during the last integlaciation (MIS 5e). *Quaternary Science Reviews*, 26, 2090-2112.

Hearty, P.J., O'Leary, M.J., Raymo, M.E., Rovere, A., Inglis, J., Roberts, D., & Bergh, E. (2012). New geological estimates of Pliocene sea levels from the Western and Northern Cape Provinces, Republic of South Africa. Abstract OS31C-1741 presented at 2012 Fall Meeting, AGU, San Francisco.

Hearty, P.J., Raymo, M.E., O'Leary, M.J., Rovere, A., Inglis, J. & Roberts, D. (2013). Extracting Plio-Pleistocene sea-level history: A diversified field approach. PALSEA Workshop, p. 19, Rome, Italy, Oct 21-25, 2013.

Hearty, P.J., Raymo, M.E., Sandstrom, M., Rovere, A., & O'Leary, M.J. (2016). Timing and estimates of Plio-Pleistocene sea-level highstands from the Republic of South Africa (RSA). European Geosciences Union, General Assembly, 17-22 April 2016. Vienna, Austria. Abstract #288099.

Hearty, P.J., Rovere, A. Sandstrom, M.R., O'Leary, M.J., Roberts, D., Raymo, M.E. (2019): Elevation measurements, sea level interpretations and dating details for South Africa Pliocene sites. *PANGAEA*, https://doi.org/10.1594/PANGAEA.910120

Hendey, Q.B. (1981a). Palaeoecology of the late Tertiary fossil occurrences in "E" Quarry, Langebaan Road, South Africa, and a reinterpretation of their geological context. *Annals of the South African Museum,* 84, 1–104.

Hendey, Q.B. (1981b). Geological succession at Langebaanweg, Cape Province, and global events of the late Tertiary. *South African Journal of Science*, 77, 33–38.

Hendey, Q.B. (1983). Palaeoenvironmental implications of the Late Tertiary vertebrate fauna of the Fynbos region. In: Deacon, H.J., Hendey, Q.B., Lambrechts, J.J.N. (Eds.), Fynbos Palaeoecology: A Preliminary Synthesis. *South African National Scientific Programmes Report*, 75, 100–115.

Hill, D.F. (2016). Spatial and Temporal Variability in Tidal Range: Evidence, Causes, and Effects. *Current Climate Change Reports*, 232–241. doi: 10.1007/s40641-016-

Hill, D. F., S. D. Griffiths, W. R. Peltier, B. P. Horton, and T. E. Törnqvist (2011). High-resolution numerical modeling of tides in the western Atlantic, Gulf of Mexico, and Caribbean Sea during the Holocene. *Journal of Geophysical Research: Oceans* 116, C10.

Jacobs, Z. & Roberts, D. L. (2009). Last interglacial age for aeolian and marine deposits and the Nahoon fossil human footprints, Southeast Coast of South Africa. Quaternary Geochronology, 4 160-169. doi: 10.1016/j.quageo.2008.09.002.

James, N.P., Bone, Y., Carter, R.M., & Murray-Wallace, C.V. (2006). Origin of the Late Neogene Roe Plains and their calcarenite veneer: Implications for sedimentology and tectonics in the Great Australian Bight. *Australian Journal of Earth Sciences*, 53(3), 407–419.

Jónsson, H., Schubert, M., Seguin-Orlano, A., Ginolhac, A., Petersen, L., Fumagalli, M. *et al.* (2014). Speciation with gene flow in equids despite extensive chromosomal plasticity. *Proceedings of the National Academy of Science*, 111, 52 | 18655–18660, doi/10.1073/pnas.1412627111.

Khan, N.S., Horton, B.P., Engelhart, S., Rovere, A., Vacchi, M., Ashe, E.L., Törnqvist, T.E., Dutton, A., Hijma, M.P., Shennan, I., 2019. Inception of a global atlas of sea levels since the Last Glacial Maximum. *Quaternary Science Reviews* 220, 359–371. https://doi.org/10.1016/j.quascirev.2019.07.016

Kaufman, D.S. & Brigham-Grette, J. (1993). Aminostratigraphic correlations and paleotemperature implications, Pliocene–Pleistocene high-sea-level deposits, northwestern Alaska. *Quaternary Science Reviews*, 12, 21–33.

Kendrick, G.W., Wyrwoll, K.H., & Szabo, B.J. (1991). Pliocene-Pleistocene coastal events and history along the western margin of Australia. *Quaternary Science Reviews*, 10(5), 419–439.

Kennedy, D. M. (2015). Where is the seaward edge? A review and definition of shore platform morphology. *Earth-science reviews*, 147, 99-108.

Kopp, R.E., Simons, F.J., Mitrovica, J.X., Maloof, A.C., & Oppenheimer, M. (2009). Probabilistic assessment of sea level during the last interglacial stage, *Nature*, 462, 863-867.

Kounov, A., Niedermann, S., De Wit, M.J., Codilean, A.T., Viola, G., Andreoli, M. & Christl, M. (2015). Cosmogenic 21Ne and 10Be reveal a more than 2 Ma alluvial fan flanking the Cape Mountains, South Africa. *South African Journal of Geology*, 118(2), pp.129-144

Krige, A.V. (1927). An examination of the Tertiary and Quaternary changes of sea-level in South Africa, with special stress on the evidence in favour of a recent world-wide sinking of ocean-level. *Annals of the University of Stellenbosch*, 5, 1-81.

Laborel, J. & Laborel-Deguen, F. (2005). Sea-Level Indicators, Biologic - *Encyclopedia of Coastal Science*. *In:* Schwartz M (ed) Encyclopedia of Coastal science. Wiley, 833–834.

Lorscheid, T., Felis, T., Stocchi, P., Obert, J.C., Scholz, D., Rovere, A., (2017). Tides in the Last Interglacial: Insights from notch geometry and palaeo tidal models in Bonaire, Netherland Antilles. *Science Reports* 7, 1–9. doi: 10.1038/s41598-017-16285-6

Lorscheid, T., & Rovere, A. (2019). The indicative meaning calculator – quantification of paleo sea-level relationships by using global wave and tide datasets. *Geospatial Data, Software and Standards* 4, 10. doi: 10.1186/s40965-019-0

Li, D., Shields-Zhou, G. A., Ling, H.-F., & Thirlwall, M. (2011). Dissolution methods for strontium isotope stratigraphy: Guidelines for the use of bulk carbonate and phosphorite rocks. *Chemical Geology*, 290(3-4), 133–144. http://doi.org/10.1016/j.chemgeo.2011.09.004

Lindsay, E.H., Opdyke, N.D., & Johnson, N.M. (1980). Pliocene dispersal of the horse *Equus* and late Cenozoic mammalian dispersal events. *Nature*, 287, 135-138.

Lisiecki, L.E., & Raymo, M.E. (2005). A Pliocene-Pleistocene stack of 57 globally distributed benthic $\delta^{18}O$ records, *Paleoceanography*, 20, PA1003, doi:10.1029/2004PA001071.

Marker, M.E., & Holmes, P.J., (2010) The geomorphology of the Coastal Platform in the southern Cape, South African Geographical Journal, 92:2, 105 116, DOI: 10.1080/03736245.2010.522041

McArthur J.M., Howarth R.J. & Shield, G.A. (2012). Chapter 7: Strontium Isotope Stratigraphy. In: The Geologic Time Scale, 2012. Gredstein FM, Ogg J.G., Schmotz M.D. and Ogg G.M. Elsevier, Vol 1 of 2, 1144 pp. LOWESS Table 5.

McArthur, J.M. (1994). Recent trends in strontium isotope stratigraphy. *Terra Nova*, 6, 331-358.

Monastersky, R. (2013). Global carbon dioxide levels near worrisome milestone. *Nature* 497, 13.

Milne, G.A., & Mitrovica, J.X., (2008). Searching for eustasy in deglacial sea-level histories. *Quaternary Science Reviews*, 27, 2292–2302.

Moucha, R., Forte, A. M., Mitrovica, J. X., Rowley, D. B & Quéré, S. (2008). Dynamic topography and long-term sea-level variations: There is no such thing as a stable continental platform. *Earth and Planetary Science Letters*, 271, 101–108.

Naish, T., Powell, R., Levy, R., Wilson, G., Scherer, R., Talarico, F., Krissek, L., et al. (2009). Obliquity-paced Pliocene West Antarctic ice sheet isolations. *Nature* 458 (7236), 322-328.

O'Leary, M.J., Hearty, P.J., Thompson, W.G., Mitrovica, J.X., Raymo, M.E., & Webster, J. M. (2013). Ice sheet collapse following a prolonged period of stable sea level during the last interglacial. *Nature Geoscience*, 28 July 2013 | doi:10.1038/ngeo1890.

Olson, S.L., & Hearty, P.J. (2009). A sustained +21 m highstand during MIS 11 (400 ka): direct fossil and sedimentary evidence from Bermuda. *Quaternary Science Reviews* 28, 271-285.

Pagani, M., Liu, Z.H., LaRiviere, J. & Ravelo, A.C. (2010). High Earth-system climate sensitivity determined from Pliocene carbon dioxide concentrations. *Nature Geoscience*, 3, 27–30.

Pether, J. (1986a). Upper Tertiary and early Quaternary marine deposits of the Namaqualand coast, Cape Province: new perspectives. *South African Journal of Science*, 82, 464-470.

Pether, J. (1986b). Late Tertiary and early Quaternary marine deposits of the Namaqualand coast, Cape Province: new perspectives. *South African Journal of Science*, 82, 464-470.

Pether, J. (1994a). Molluscan evidence for enhanced deglacial advection of Agulhas water in the Benguela Current, off southwestern Africa. *Palaeogeography, Palaeoclimatology, Palaeoecology*, 111, 99–117.

Pether, J. (1994b). The sedimentology, palaeontology and stratigraphy of coastal-plain deposits at Hondeklip Bay, Namaqualand, South Africa. M.Sc. Thesis, University of Cape Town, South Africa, 313pp.

Pether, J., Roberts, D.L., & Ward, J. (2000). Deposits of the West Coast. *In:* Partridge, T.C., Maud, R.R. (Eds.), The Cenozoic of Southern Africa. Oxford Monographs on Geology and Geophysics, 40, 33–54.

Pickford, H. (1998). Onland Tertiary marine strata in southwestern Africa; eustacy, local tectonics and epeirogenesis in a passive continental margin. South African Journal of Science, 94, 5-8.

Pollard, D. & De Conto, R.M. (2009). Modelling West Antarctic ice sheet growth and collapse through the past five million years. *Nature* 458, 329–332.

Pollard, D., DeConto, R.M., & Alley, R.B. (2015). Potential Antarctic ice sheet retreat driven by hydrofracturing and ice cliff failure. *Earth and Planetary Science Letters*, 412, 112-121.

Raymo, M.E., Mitrovica, J.X., O'Leary, M.J., DeConto, R.M., & Hearty, P.J. (2011). Departures from eustasy in Pliocene sea-level records. *Nature Geoscience*, 4, 328–332.

Raymo, M.E., & Mitrovica, J.X. (2012). Collapse of polar ice sheets during the stage 11 interglacial. *Nature* 483, 453–456.

Roberts, D.L., 2008. Last interglacial hominid and associated vertebrate fossil trackways in coastal eolianites, South Africa. *Ichnos*, 15(3-4), pp.190-207.

Roberts, D.L., Brink, J., 2002. Dating and correlation of Neogene coastal deposits in the Western Cape, South Africa: implications for Neotectonism. *South African Journal of Geology*, 105, 337–352.

Roberts, D.L., Matthews, T., Herries, A.I.R., Boulter, C., Scott, L., Dondo, C. *et al.* (2011). Regional and global context of the Late Cenozoic Langebaanweg (LBW) palaeontological site: West Coast of South Africa. *Earth-Science Reviews*, 106, 191–214.

Roberts, D.L., Karkanas, P., Jacobs, Z., Marean, C.W. & Roberts, R.G. (2012). Melting ice sheets 400,000 yr ago raised sea level by 13 m: Past analogues for future trends. *Earth and Planetary Science Letters*, 357–358, 226–237. doi:https://doi.org/10.1016/j.epsl.2012.09.006

Roep, Th.B., and Beets, D.J. (1988). Sea-level rise and paleotidal levels from sedimentary structures in the coastal barrier of the western Netherlands since 5600 B.P., *Geologie en Mijnbouw*, 67 (1), 53-60.

Rogers, A.W. (1905). An Introduction to the Geology of the Cape Colony. Longmans, Green and Co, London, UK. 463 pp.

Rovere, A. (2020). Paleo Sea Level Utilities (Version 1.1). Zenodo. http://doi.org/10.5281/zenodo.3689427

Rovere, A., Raymo, M.E., Mitrovica, J.X., Hearty, P.J., O'Leary, M.J., & Inglis, J.D. (2014). The Mid-Pliocene sea-level conundrum: Glacial isostasy, eustasy and dynamic topography. *Earth and Planetary Science Letters*, 387, 27–33.

Rovere, A., Hearty, P.J., Austermann, J., Mitrovica, J.X., Gale, J., Moucha, R., Forte, A.M., & Raymo, M.E. (2015). Mid-Pliocene shorelines of the US Atlantic Coastal Plain — An

improved elevation database with comparison to Earth model predictions. *Earth Science Reviews*, 145, 117–131. doi:10.1016/j.earscirev.2015.02.007

Rovere, A., Raymo, M.E., Vacchi, M., Lorscheid, T., Stocchi, P., Gómez-Pujol, L., Harris, D.L., Casella, E., O'Leary, M.J., & Hearty, P.J. (2016). The analysis of Last Interglacial (MIS 5e) relative sea-level indicators: Reconstructing sea-level in a warmer world. *Earth Science Reviews*, 159, 404–427. doi:10.1016/j.earscirev.2016.06.006

Rovere, A., Casella, E., Harris, D.L., Lorscheid, T., Nandasena, A.K., Dyer, B. *et al.* (2017). Giant boulders and Last Interglacial storm intensity in the North Atlantic. *Proceedings of the National Academy of Science,* 114:201712433. doi: 10.1073/pnas.1712433114

Rovere, A., Casella, E., Harris, D.L., Lorscheid, T., Nandasena, A.K., Dyer, B. *et al.* (2018). Reply to Hearty and Tormey: Use the scientific method to test geologic hypotheses, because rocks do not whisper. *Proceedings of the National Academy of Science,* 201800534. doi: 10.1073/pnas.1800534115

Rudge, J. F., Roberts, G. G., White, N. J., and Richardson, C. N. (2015). Uplift histories of Africa and Australia from linear inverse modeling of drainage inventories. *Journal of Geophysical Research: Earth Surface,* 120, 894–914, doi:10.1002/2014JF003297.

Sandstrom, R.M., Cai, Y., Raymo, M.E., Goldstein, S.L., Inglis, J.D., & Mata, R. (2014). Determining Effects of Diagenesis on Geochemical Dating of Plio-Pleistocene Shallow Marine Fauna. In: Program with Abstracts, American Geophysical Union (AGU), Annual National Meeting in San Francisco, CA. December 17th, 2014. Poster Presentation.

Shen G.T., Campbell T.M., Dunbar R.B., Wellington G.M., Colgan M.W. & Glynn P.W. (1991). Paleochemistry of manganese in corals from the Galapagos Islands. *Coral Reefs*. 10, 91–100.

Shennan, I., Long, A.J., & Horton, B.P., 2015. Handbook of Sea-level Research. Wiley Online Library.

Shennan, I., 1982. Interpretation of Flandrian sea-level data from the Fenland, England. *Proceedings of the Geologists' Association*, 93(1), pp.53-63.

Sisser, W.G., and Dingle, R.V., 1981. Tertiary Sea-Level movements around southern Africa. *Journal of Geology*, 89 (4), 523-536.

Spasojevic, S. & Gurnis, M. (2012). Sea level and vertical motion of continents from dynamic earth models since the Late Cretaceous. *American Association of Petroleum Geology Bulletin*, 96(11), 2037-2064.

Stap, L.B., Boer, B., Ziegler, M., Bintanja, R., Lourens, L.J., van de Wal, S.W. *et al.* (2016). CO_2 over the past 5 million years: Continuous simulation and new δ^{11}B-based proxy data. *Earth and Planetary Science Letters*, 439, 1-10.

Stocchi, P., Vacchi, M., Lorscheid, T., de Boer, B., Simms, A.R., van de Wal, R.S., Vermeersen, B.L., Pappalardo, M. and Rovere, A. (2018). MIS 5e relative sea-level changes

in the Mediterranean Sea: Contribution of isostatic disequilibrium. *Quaternary Science Reviews*, 185, pp.122-134.

Stollhofen, H., Stanistreet, I.G., von Hagke, C. & Nguno, A. (2014). Pliocene–Pleistocene climate change, sea level and uplift history recorded by the Horingbaai fan-delta, NW Namibia. *Sedimentary Geology*, 309, 15-32.

Trenhaile, A. (2014). Modelling the effect of Pliocene–Quaternary changes in sea level on stable and tectonically active land masses. *Earth Surface Processes and Landforms*, 39(9), pp.1221-1235.

Van de Plassche, O. (1986). Sea-level Research: A Manual for the Collection and Evaluation of Data. Geobooks, Norwich.

Walford, H. L., and N. J. White, N.J., (2005). Constraining uplift and denudation of west African continental margin by inversion of stacking velocity data. *Journal of Geophysical Research*, 110, B04403, doi:10.1029/2003JB002893.

Wessel, P. & Smith, W. H. F. (1996). A global, self-consistent, hierarchical, high-resolution shoreline database, *Journal of Geophysical Research*, 101(B4), 8741–8743.

Wilmes, S.B., Green, J.M., Gomez, N., Rippeth, T.P. & Lau, H. (2017). Global Tidal Impacts of Large-Scale Ice Sheet Collapses. *Journal of Geophysical Research: Oceans*, 122(11), pp.8354-8370.

Zhu, B.Q., (2016). A Review on Late Quaternary Environmental Change in the Namibia, South-Western Africa. *Journal of Earth Science and Climate Change*, 7, 348. doi:10.4172/2157-7617.1000348

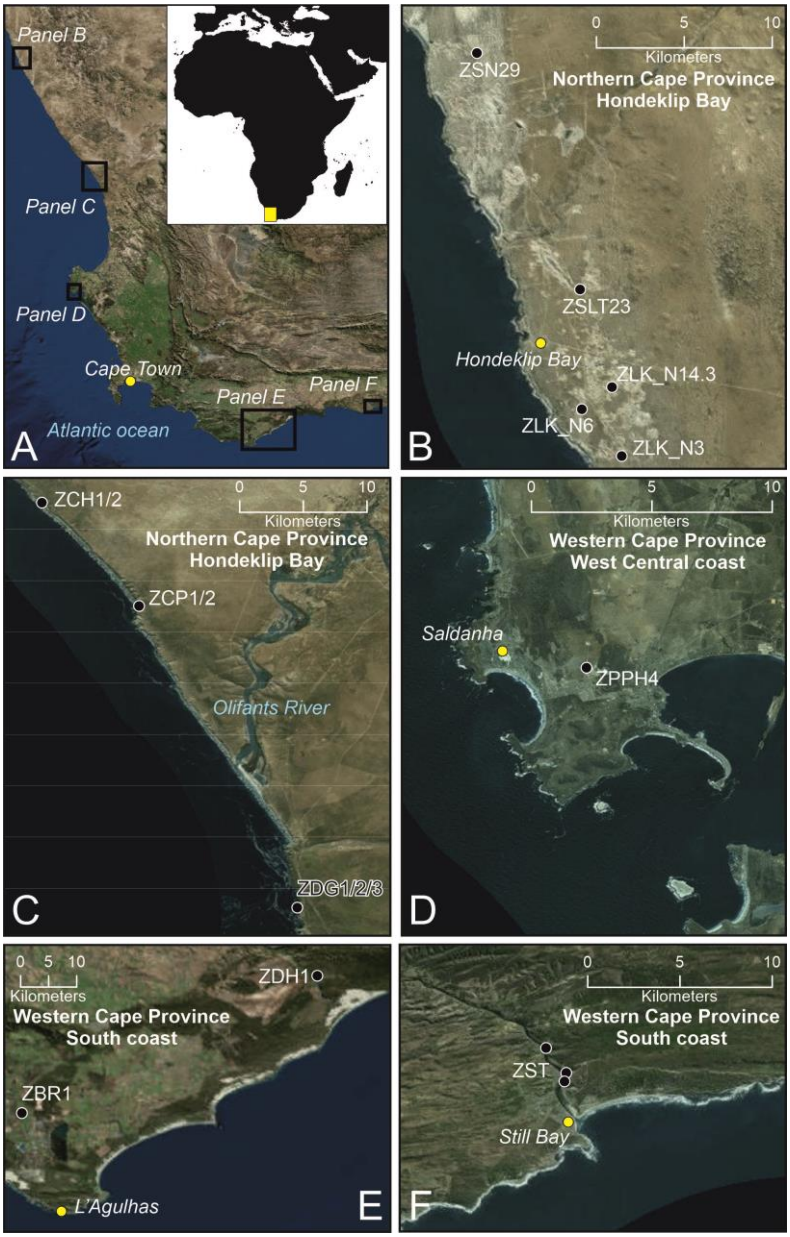

Figure 1. (A) Study area, with location of sub-regions discussed in the text (panels B-F). Upper right inset: location of the study area within a larger geographic context. Background imagery source: Esri, DigitalGlobe, GeoEye, i-cubed, USDA FSA, USGS, AEX, Getmapping, Aerogrid, IGN, IGP, swisstopo, and the GIS User Community. Inset in A was drawn from Global Self-Consistent Hierarchical High-resolution Geography, GSHHG. Version 2.3.7 June 15, 2017 (Wessel et al., 1996).

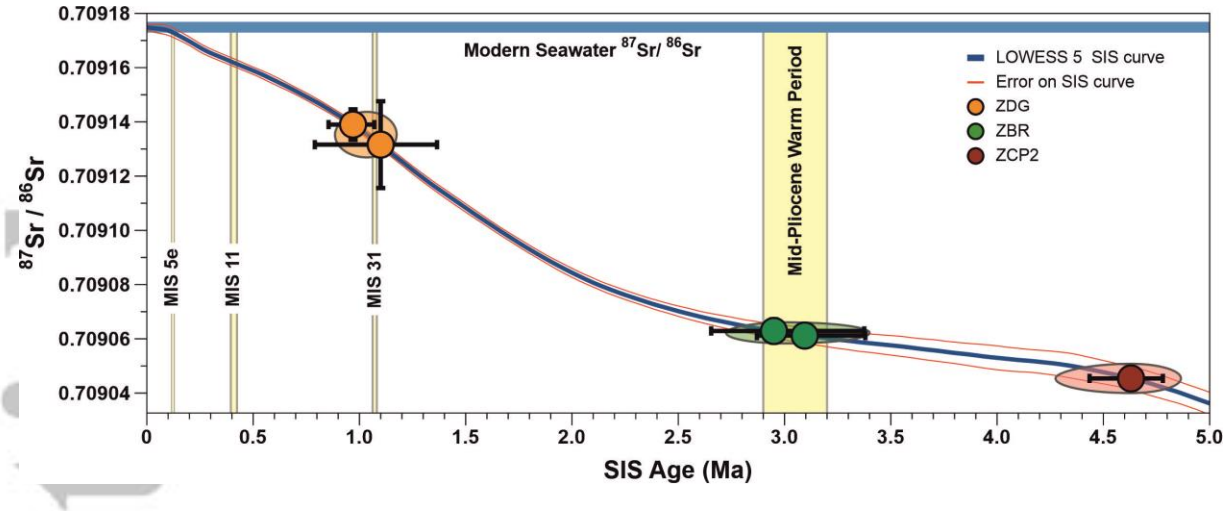

Figure 2. Sr isotope stratigraphy (SIS) ages from the best-preserved bivalves on three different terraces in RSA. Colored circles with black error bars are based on individual shell averages (from an average of inner leach individual filaments) with errors based on 2σ standard error of the mean of those filaments. Shaded ellipses (behind circles) are terrace ages derived from averages of all screened sample filaments. The size of the ellipse is based on combined uncertainty from 2σ SEM of sample filaments and LOWESS SIS curve error. Yellow bars are exceptionally warm periods and interglacials where sea level is thought to be the same or higher than present (Lisiecki and Raymo, 2005; Dutton et al., 2015; de Wet et al., 2016).

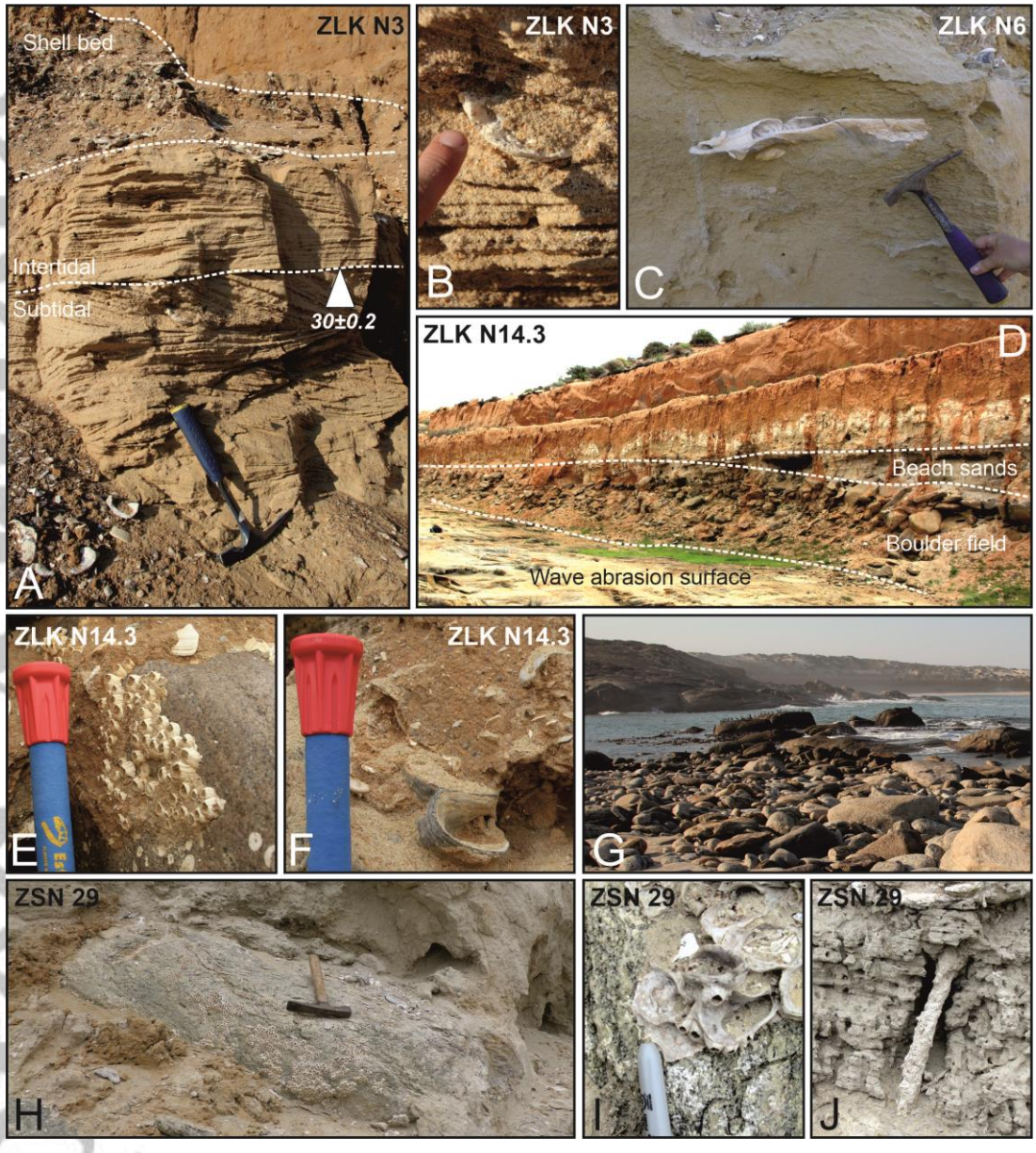

Figure 3. Details of stratigraphic sections surveyed along the Northern Cape Province – Hondeklip Bay area. **(A)** Subtidal-intertidal contact at ZLK_N3. **(B)** Detail of the subtidal deposit in A; **(C)** Large *Ostrea* shell at ZLK_N6. **(D)** Stratigraphy of site ZLKN_14.3, showing an imbricated boulder pavement deposited on a wave abrasion surface, capped by beach sands and terrigenous deposits. **(E, F)** Details of D, showing barnacles (E) and oysters (F) in living position on the boulders. (**G**) Modern boulder pavement provides an analog of site ZLKN_14.3 and several other sites. **(H)** Boulder at site ZSN29, with fossil barnacles attached. **(I)** Overgrowth of barnacles on oysters at site ZSN29. **(J)** Ophiomorpha burrows at site ZSN29.

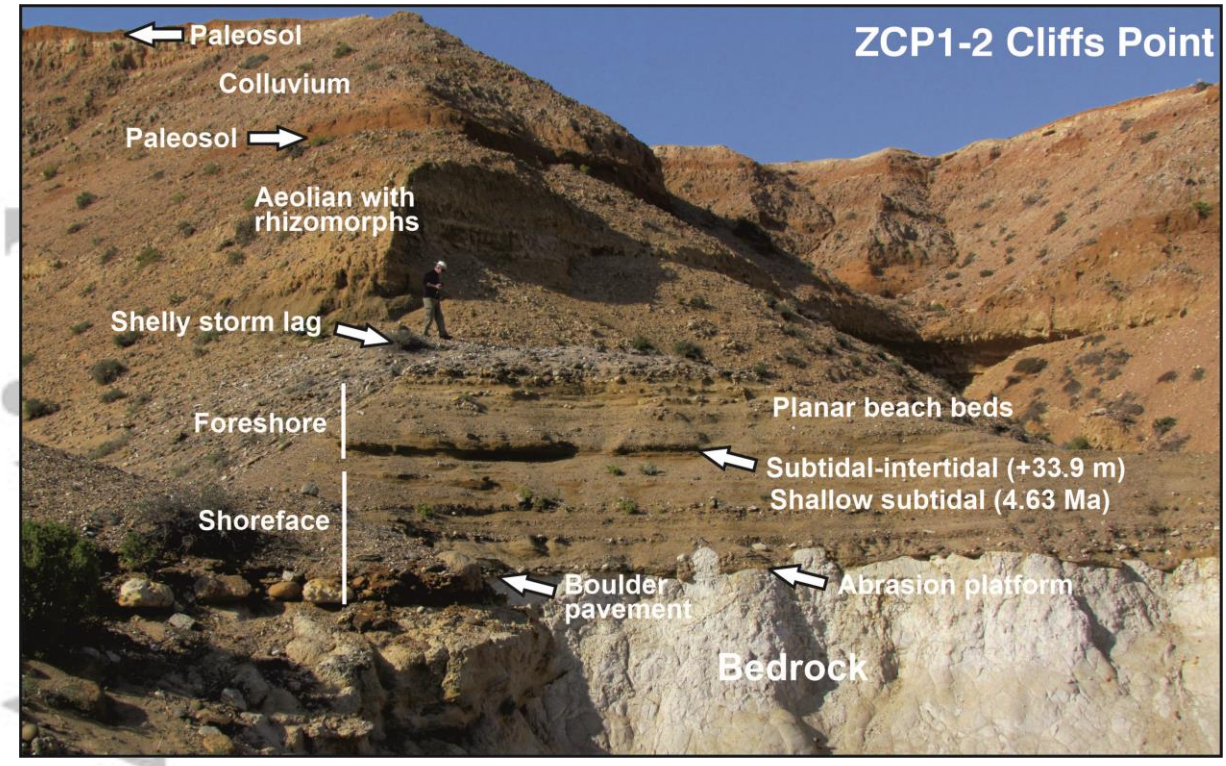

Figure 4. Annotated photo of key ZCP1-2 with labels of various physical boundaries and representative sedimentary shoreline facies, rising from bedrock abrasion platform to soils. Refer to Table 1 for corresponding information on RSL indicators.

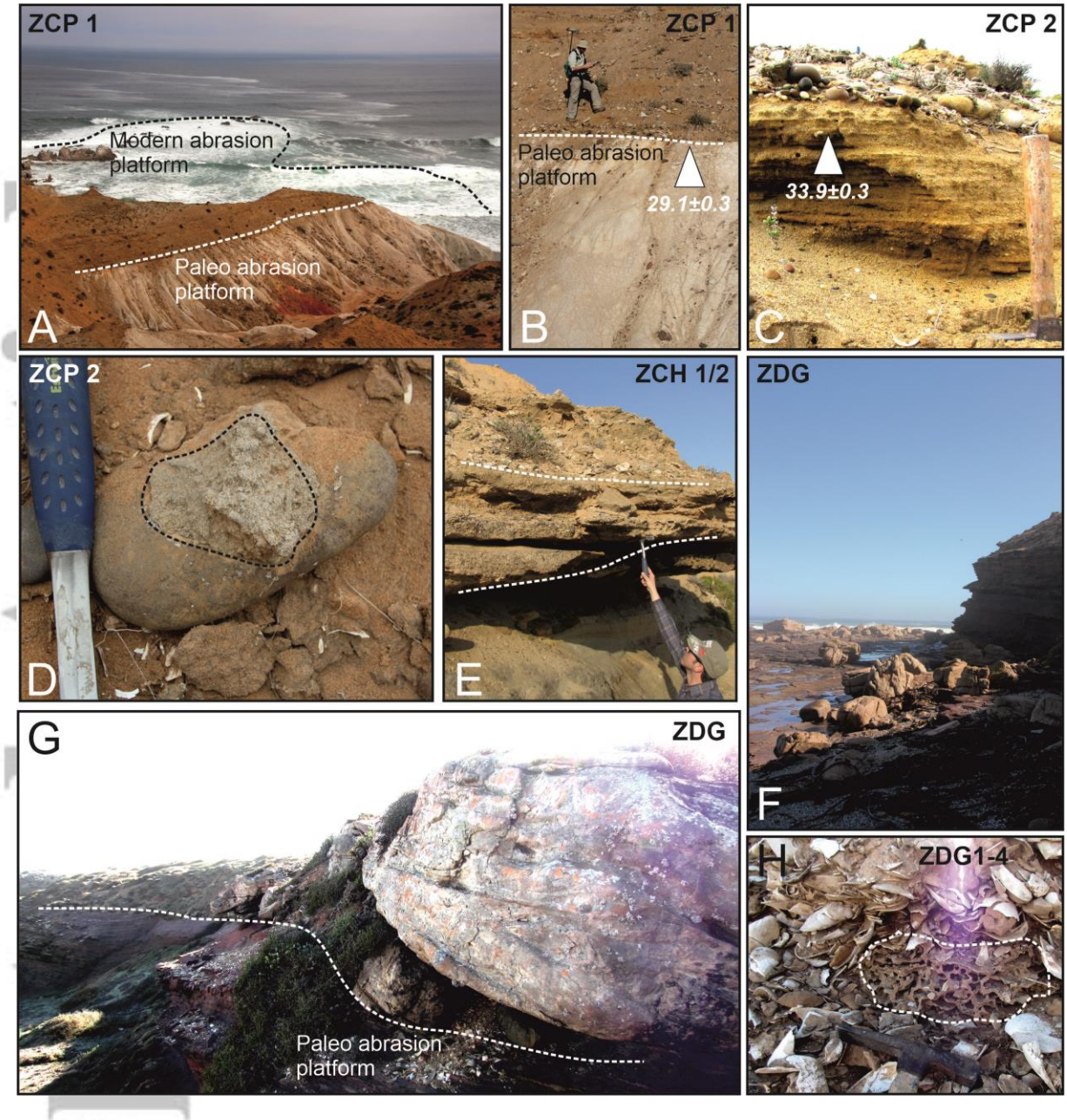

Figure 5. Details of stratigraphic sections surveyed in the Northern Cape Province - Olifants River mouth area **(A)** Modern and paleo abrasion platforms at site ZCP1. **(B)** Detail of the abrasion platform at ZCP1. **(C)** Transition between subtidal beds and cobble-shell deposit at ZCP2. **(D)** Encrusting marine calcareous algae on cobbles at ZCP2. **(E)** Sandy-pebbly layers at ZCH1/2. **(F)** Modern abrasion platform at ZDG. **(G)** Paleo abrasion platform at ZDG. **(H)** Sand with abundant rhizomorphs and fossil termite structures (dashed line) among articulated valves of *D. rogersi* at site ZDG1-4.

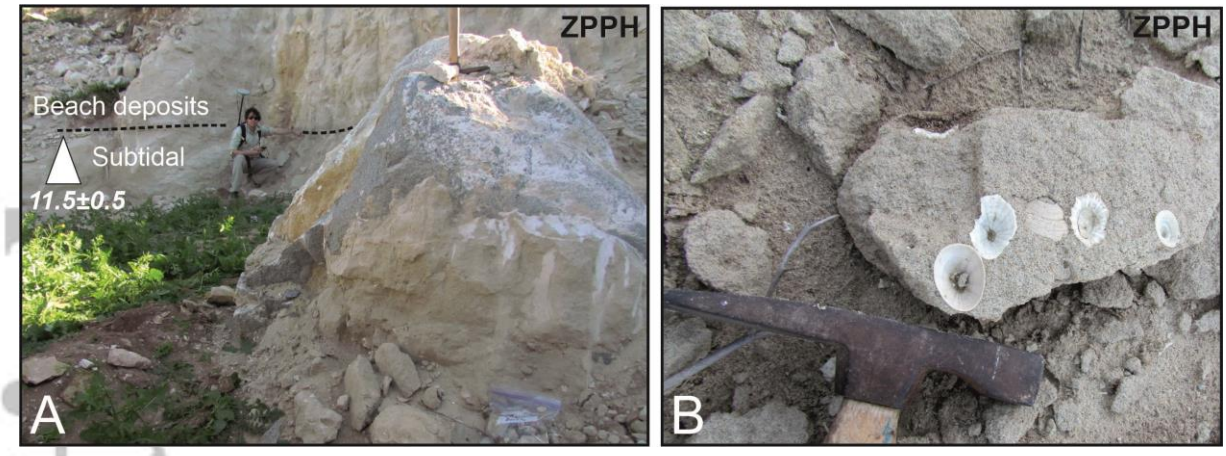

Figure 6. Western Cape Province - West Central coast area. **(A)** Overview of the site ZPPH with subtidal-beach transition at +11.5 ± 0.5 m. **(B)** Limpets including *Fissurella* broken from the boulder surface at ZPPH.

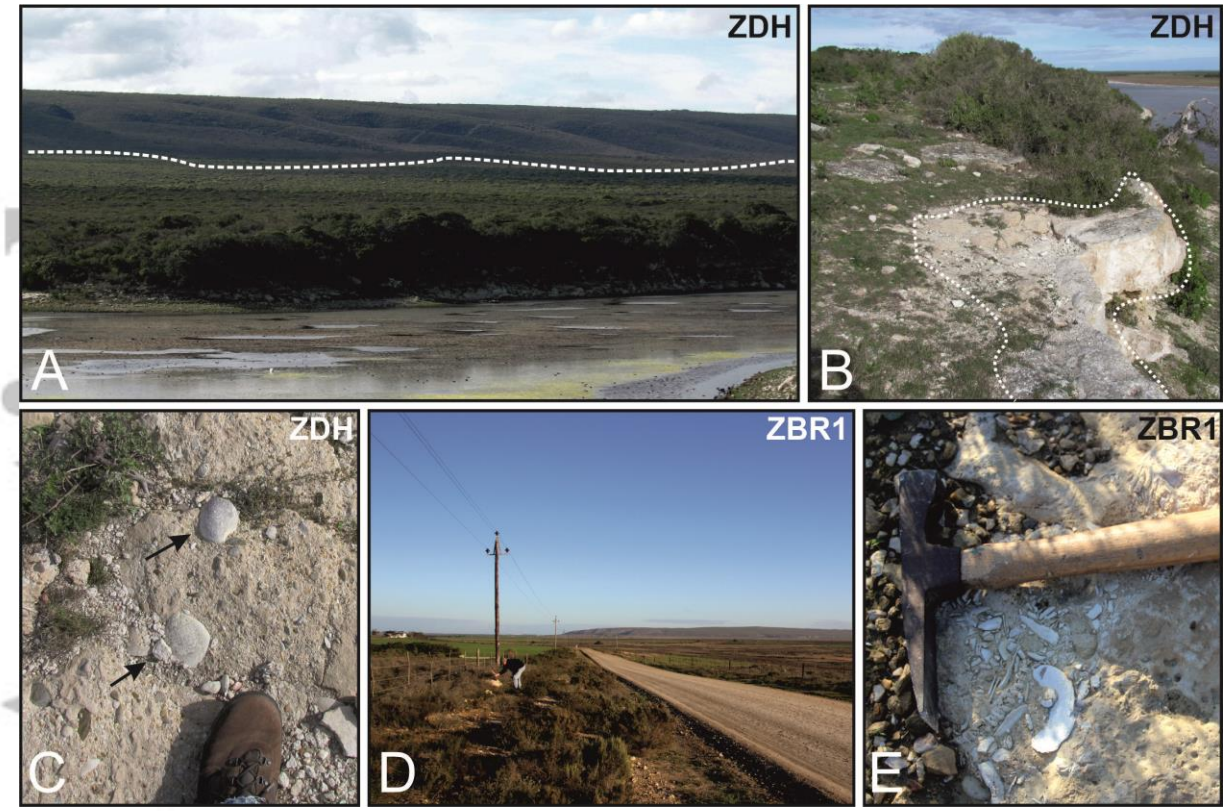

Figure 7. Western Cape Province - South coast area. **(A)** Long and wide Pliocene marine terrace at ZDH. The dashed line indicates the approximate inner margin. **(B)** 'caprock' composed of fossiliferous marine calcareous grainstone and bio-rudstone (dashed line) at ZDH. **(C)** large, concave-down oriented *Glycymeris* at site ZDH (arrows). **(D)** Overview of ZBR1 site. **(E)** Marine shells, many articulated in a matrix of fine marl and in variable in orientation at ZBR1, indicating deposition in a few metres of water.

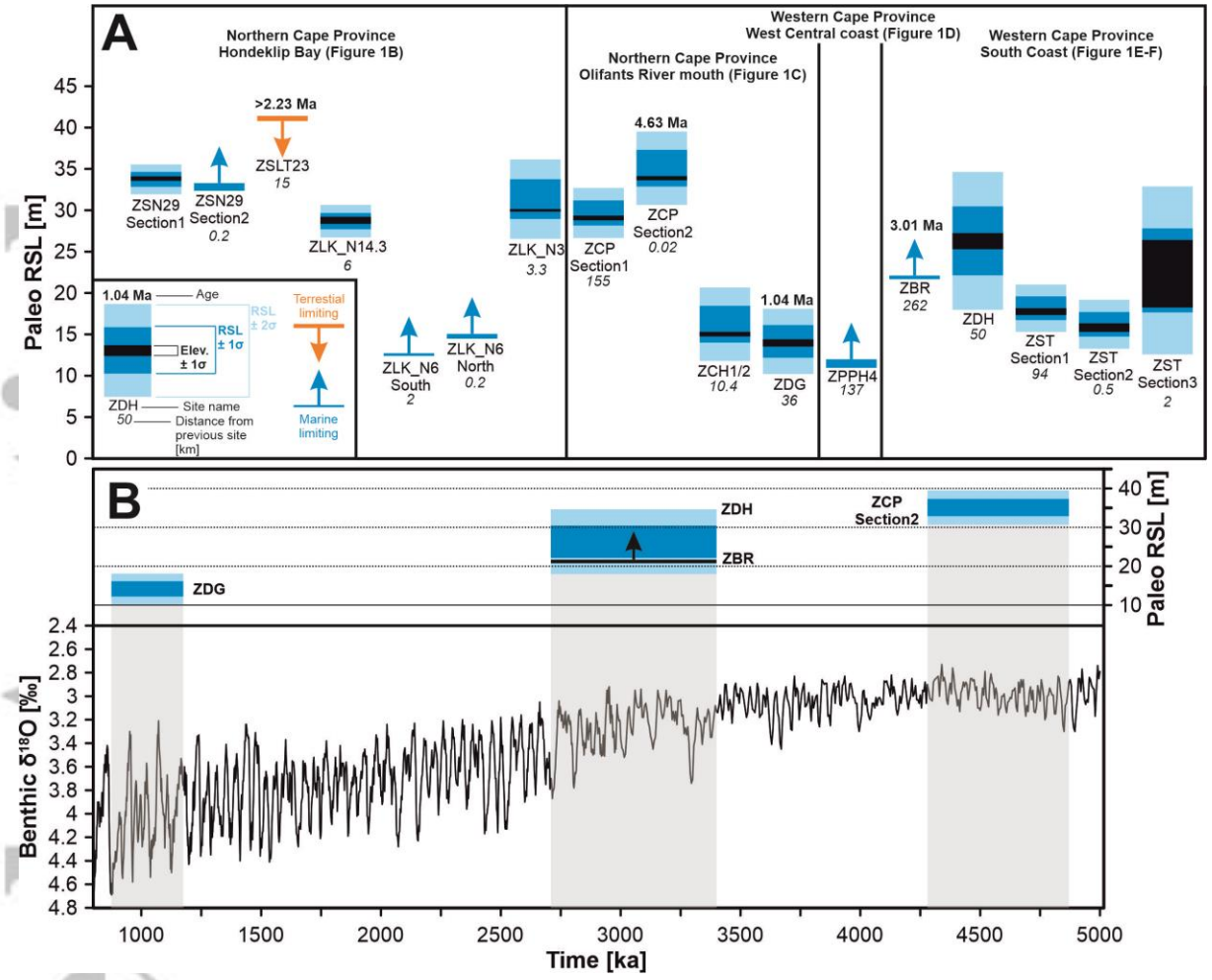

Figure 8. Overview of Plio-Pleistocene RSL indicators surveyed, interpreted and dated in this study. (**A**) Elevation and (where applicable) paleo RSL estimates for the sites described in the text (Table 2). (**B**) Lisiecki and Raymo (2005) delta ^{18}O stack compared with ages and elevations obtained in this study. The graph shows the correlation between ZDH and ZBR as per Rovere et al., 2014.

Table 1. RSL indicators surveyed this study, Reference Water Level (RWL) and Indicative Range (IR) associated to each indicator. *In the case of Donkergat (ZDG), we use the elevation of the shore platform inner margin measured in the field instead of MHHW.

RSL indicator	RWL	IR	Definitions
Shore Platform (marine abrasion platform of older bedrock)*	(MHHW + Poe)/2	MHHW - Poe	**MHHW, MLLW - Mean Higher High Water, Mean Lower Low Water.** Obtained from 19-year predictions calculated using the OTIS software (Egbert et al., 1994; Egbert and Erofeeva, 2002).
Marine geomorphic terrace/sedimentary constructional platform	(SWSH + db)/2	SWSH - db	**Ud - Upper distribution.** Upper distribution of intertidal organisms measured in the field (see Laborel and Laborel-Deguen, 2005 for a review of similar indicators).
Transition between subtidal/intertidal (or shoreface/foreshore) facies	(db + MHHW)/2	MHHW - db	**db - Breaking depth.** The depth at which significant waves interact with the bottom.
Horizontal barnacle/oyster band on cobble/boulder pavement above a shore platform	(Ud + MLLW)/2	Ud - MLLW	**Poe - Platform outer edge.** Seaward edge of a shore platform, defined by Kennedy (2015) as: "*the point where active erosion of the bedrock ceases.*" **SWSH - Storm wave swash height.** The maximum elevation reached by extreme storm waves on the beach. All values above were calculated using the IMCalc software (Lorscheid and Rovere, 2019).
Marine limiting	Ophiomorpha burrows, subtidal cross-bedding and coarse pebbles Contact between marine and terrestrial deposits Subtidal cross beds and boulder with *Patella* sp.		
Terrestrial limiting	Deposits that were surely emplaced above MHHW (e.g. high-energy storm deposits)		

Table 2. Overview of RSL indicators, their location and quantification of indicative meaning (Reference Water Level, RWL and Indicative Range, IR). The paleo RSL uncertainty column includes an additional 20% uncertainty that accounts for possible difference in tidal and wave parameters since the Pliocene. *At this site it was not possible to achieve a fix to the Omnistar satellites, hence the accuracy of the vertical measurement is greatly reduced (4.1m, ±1σ).

Site Code	Section	Geographic name	RSL indicator (see Table 1 for quantification of the indicative meaning)	Lat [deg]	Lon [deg]	Elevation [m]	Elevation error [m] ±1σ	RWL [m]	IR [m]	Paleo RSL [m]	Paleo RSL uncertainty [m] ±1σ
Northern Cape Province – Hondeklip Bay											
ZSN29	Section 1	Somnaas	Horizontal barnacle/oyster band on cobbles/boulders above a shore platform	-30.1699	17.24864	33.8	0.3	0.1	1.4	33.7	0.9
ZSN29	Section 2	Somnaas	Ophiomorpha burrows, subtidal cross-bedding and coarse pebbles	-30.1707	17.2504	32.8	0.5	Marine limiting			
ZSLT23		Koingnass	Storm deposit	-30.2927	17.30492	41.1	0.3	Terrestrial limiting			
ZLK_N14.3		Langklip	Horizontal barnacle/oyster band on cobbles/boulders above a shore platform	-30.3417	17.318	28.8	0.4	0.1	1.4	28.7	1
ZLK_N6	Section South	Langklip	Contact between marine and terrestrial deposits	-30.3543	17.30043	14.8	0.3	Marine limiting			
ZLK_N6	Section North	Langklip	Contact between marine and terrestrial deposits	-30.3532	17.30255	12.6	0.2	Marine limiting			
ZLK_N3		Langklip	Transition between subtidal/intertidal (or shoreface/foreshore) facies	-30.3772	17.32301	30.0	0.2	-1.4	4	31.4	2.4
Northern Cape Province – Olifants River mouth											

ZCP	Section 1	Cliff Point	Shore Platform (marine abrasion platform of older bedrock)	-31.5874	18.11939	29.1	0.3	-0.6	2.5	29.7	1.5
ZCP	Section 2	Cliff Point	Transition between a subtidal (Upper shoreface) to intertidal facies	-31.5873	18.11962	33.9	0.3	-1.2	3.7	35.1	2.2
ZCH	Section 1/2	Channel	Transition between a subtidal (Upper shoreface) to intertidal facies	-31.5141	18.05109	15.0	0.3	-1.2	3.7	16.2	2.2
ZDG	Section 4	Donkergat	Shore Platform (marine abrasion platform of older bedrock)	-31.8014	18.23132	14.0	0.4	-0.2	3.2	14.2	2.0
Western Cape Province – West Central coast											
ZPPH		Prospect Hill	Subtidal cross beds and boulder with *Patella sp.*	-33.0012	17.91995	11.5	0.5	Marine limiting			
Western Cape Province – South coast											
ZBR		Breasdorp	Subtidal sediments	-34.6748	19.9245	21.9	0.2	Marine limiting			
ZDH		De Hoop	Sediments deposited in the swash zone	-34.4544	20.39775	26.3	1.0	0.0	6.7	26.3	4.2
ZST	Section1	Still Baai	Shore Platform (marine abrasion platform of older bedrock)	-34.3559	21.41832	17.8	0.4	-0.4	2.2	18.2	1.4
ZST	Section2	Still Baai	Shore Platform (marine abrasion platform of older bedrock)	-34.36	21.41741	15.8	0.5	-0.4	2.2	16.2	1.5
ZST*	Section3	Still Baai	Shore Platform (marine abrasion platform of older bedrock)	-34.3437	21.40838	22.3	4.1	-0.4	2.2	22.7	5.1

Table 3. Summary of SIS ages obtained from the samples collected in this study. For more detailed metadata regarding each sample, please refer to the SESAR IGSN ID (http://www.geosamples.org/). [a] Leach variation score is based on total leach variation (ppm) of initial vs. inner leaches, with <11 ppm = "1," 11-17 ppm = "2," and >17ppm = "3."; [b] Samples with an average preservation score ≥ "2" are considered unreliable and not included in terrace age calculations; [c] Samples with ≥ 3 filament measurements have age uncertainties calculated as 2σ SEM (bolded), samples with less (italics) have uncertainty based on 2σ of external standard NBS987; [d] Terrace ages based on averging inner leach filaments from samples that passed our screening criteria (preservation score < 2); [e] Total uncertainty is based oncombining the 2σ SEM of sample filaments and lowess SIS curve uncertainties. This is the error used in calculating terrace ages; N.A. - Not measured.

Sample Metadata			**Preservation Index**					**Sr isotope stratigraphy ages**						
Sample Name	**SESAR ISGN ID**	**Bivalve Classification**	**Optical Score**	**SEM Score**	**T.E. Scores (Mg/Mn/Fe)**	**Leach Variation Score[a]**	**Preservation Score (Avg.)**	**n (filaments)**	**$^{87}Sr/^{86}Sr$ (Corr. 987)**	**2σ Error[c]**	**Shell Leach Variation (ppm)**	**Mean SIS Age (Ma)**	**Max SIS Age (Ma)**	**Min SIS Age (Ma)**
ZBR1-A	IEMRS003Z	*Glycyermis sp.*	1	1	1.0	1	**1.0**	4	0.7090612	**0.0000027**	1.11	**3.10**	3.38	2.87
ZBR1-D	IEMRS0042	*Ostrea sp.*	1	1	1.3	1	**1.1**	6	0.7090629	**0.0000043**	3.62	**2.95**	3.38	2.66
ZDH1-C (Z3-C)	IEMRS0046	*Glycyermis sp.*	2	N.A.	N.A.	2	**2.0[b]**	1	0.7090837	*0.0000079*	10.99	**2.02**	2.27	1.83
ZCP2-B	IEMRS004P	*Ostrea sp.*	2	2	2.0	1	**1.8**	4	0.7090454	**0.0000033**	5.86	**4.63**	4.78	4.44
ZCP2-E	IEMRS004S	*Ostrea sp.*	2	2	2.0	N.A.	**2.0[b]**	2	0.7090997	*0.0000126*	N.A.	**1.67**	1.94	1.43
ZDG4a-A	IEMRS004A	*Donex sp.*	1	1	1.0	N.A.	**1.0**	3	0.7091390	**0.0000056**	N.A.	**0.97**	1.07	0.86
ZDG4b-C	IEMRS004I	*Dosinia sp.*	1	2	1.3	2	**1.6**	3	0.7091316	**0.0000160**	11.48	**1.10**	1.37	0.79
ZSLT23	IEMRS004W	*Ostrea sp.*	3	2	2.3	3	**2.6[b]**	2	0.7090643	*0.0000126*	44.94	**2.85**	4.19	2.23
Average terrace SIS age[d]														

Site Code	Elevation (msl)	Location	Preservation Score (Avg.)	n samples	n filaments	$^{87}Sr/^{86}Sr$ (Corr. 987)	2σ SEM (sample)	2σ Total Uncertainty[e]	Mean SIS Age (Ma)	Max SIS Age (Ma)	Min SIS Age (Ma)
ZBR	21.90 ± 0.20	Breasdorp	1.1	2	**10**	**0.7090622**	0.0000027	0.0000039	**3.01**	3.40	2.73
ZDG	13.96 ± 0.43	Donkergat	1.3	2	**6**	**0.7091353**	0.0000082	0.0000084	**1.04**	1.18	0.88
ZCP2	33.70 ± 0.29	Cliff Point	1.8	1	**4**	**0.7090454**	0.0000033	0.0000054	**4.63**	4.87	4.28